creative commons

COMMONS DEED

저작자표시-비영리-변경금지 2.0 대한민국

이용자는 아래의 조건을 따르는 경우에 한하여 자유롭게

- 이 저작물을 복제, 배포, 전송, 전시, 공연 및 방송할 수 있습니다.

다음과 같은 조건을 따라야 합니다:

저작자표시. 귀하는 원저작자를 표시하여야 합니다.

비영리. 귀하는 이 저작물을 영리 목적으로 이용할 수 없습니다.

변경금지. 귀하는 이 저작물을 개작, 변형 또는 가공할 수 없습니다.

- 귀하는, 이 저작물의 재이용이나 배포의 경우, 이 저작물에 적용된 이용허락조건을 명확하게 나타내어야 합니다.
- 저작권자로부터 별도의 허가를 받으면 이러한 조건들은 적용되지 않습니다.

저작권법에 따른 이용자의 권리는 위의 내용에 의하여 영향을 받지 않습니다.

이것은 이용허락규약(Legal Code)을 이해하기 쉽게 요약한 것입니다.

Disclaimer

dCollection

약학박사학위논문

Rational Design and Engineering of Interferon-β 1a for Improving Biophysical and Pharmacokinetic Properties

합리적 설계에 따른 단백질 공학을 통한

인터페론 베타의 생·물리학적 성질 및

약동력학적 성질의 개선

2014 년 8 월

서울대학교 대학원

약학과 병태생리학 전공

송 경

ABSTRACT

Rational Design and Engineering of Interferon-β 1a for Improving Biophysical and Pharmacokinetic Properties

Kyoung Song

College of Pharmacy

The Graduate School

Seoul National University

Recombinant human IFN-β 1a (rhIFN-β 1a) is a single glycosylated protein (at N80, 1N) with anti-viral, anti-proliferation, and immunomodulatory activities. rhIFN-β 1a has been approved as a drug for the treatment of multiple sclerosis (MS). rhIFN-β is a highly hydrophobic protein that has a strong propensity for aggregation. It was already well known that aggregation reduces the activity of rhIFN-β and can also contribute to low production yield in mammalian culture systems, resulting in the high price of therapeutics high cost of production. As with other protein drugs, rhIFN-βs also have relatively short serum half-lives that may necessitate frequent parenteral administration to achieve efficacy. The frequent injections and related local skin reactions are the most common inconveniences associated with treatment.

Modification of protein drugs by the attachment of an oligosaccharide moiety or polyethylene glycol (PEG) can improve patient compliance through sustained clinical response with less frequent dosing. This is due to the fact that glycoengineered or PEGylated protein could exhibit improved thermal stability and solubility, thus prolonging the circulating half-life. Moreover, it could reduce immunogenicity of the protein drug. To address these unmet needs by designing a biobetter version of rhIFN-β, an oligosaccharide moiety and PEG were sequentially introduced on rhIFN-β 1a.

Site-specific hyperglycosylation was introduced into rhIFN-β 1a via site-directed mutagenesis. Glycoengineered rhIFN-β 1a was characterized by western blotting, isoelectric focusing, enzyme immunoassay, and glycosylation analysis. Glycoengineering of rhIFN-β 1a resulted in the production of a new molecular entity, R27T, with which we could obtain valuable competitive intellectual property rights. Glycoengineering successfully resulted in a product that exhibited unaltered ligand-receptor binding, with no observed change in the specific activity. R27T displayed improved stability and solubility, reduced aggregation, and increased half-life in pharmacokinetic (PK) studies, suggesting that hyperglycosylated rhIFN-β could be a biobetter version rhIFN-β for the treatment of MS.

The addition of PEG is well known as an effective strategy to alter the PK profiles of a variety of drugs, thereby improving therapeutic potential. To obtain a more dramatic improvement in PK property, PEG was conjugated to R27T using several methods. PEG-R27T exhibited improved *in vivo* circulation half-lives over

their corresponding native forms, although there was little activity loss. Taken together, rational design and engineering of rhIFN-β 1a using glycoengineering and PEGylation resulted in improved biophysical and PK properties, suggesting that these modification products could serve as new improved therapeutics for MS.

Keywords: recombinant human interferon-β-1a (rhIFN-β 1a), glycoengineering, PEGylation, biobetter, multiple sclerosis (MS)

Student number: 2009-30466

CONTENTS

ABSTRACT ……... i

CONTENTS …….. iv

LIST OF TABLES……. vii

LIST OF FIGURES……... viii

LIST OF ABBREVIATIONS…… x

I. INTRODUCTION ……. 1

1. Multiple sclerosis ……..... 2
2. Therapeutics for multiple sclerosis…… 6
3. Implementation of rhIFN-β therapy for multiple sclerosis..... 9
4. Rational design and engineering of protein therapeutics…….. 11

II. PURPOSE OF THE STUDY……..... **14**

III. MATERIALS AND METHODS ……..... **16**

1. Construction of a gene encoding rhIFN-β glycosylation analogs……... 17
2. Expression of rhIFN-β construct in mammalian cells……..... 19
3. Purification and characterization of rhIFN-β mutants……..... 19
4. Analysis of expressed proteins…….…… 20

5. Glycosylation site confirmation……..... 20

6. Monosaccharide and sialic acid composition analysis …… 21

7. Oligosaccharide profiling …… 22

8. Exoglycosidase digestion……..... 23

9. Protein stability measurement by biophysical analysis ……... 23

10. Determination of antiviral activity..... 24

11. Anti-proliferation activity……... 25

12. Immunomodulatory effect……. 25

13. Molecular modeling for R27T/IFNAR2 complex…….. 26

14. PEGylation of R27T……... 27

15. Purification of PEG-R27T…….. 28

16. *In vivo* pharmacokinetic analysis in rats……. 28

17. statistical analysis……... 30

IV. RESULT…….. 31

1. Construction of rhIFN-β glycosylation analogs, R27T……..... 32

2. Development of cell line and its productivity……..... 38

3. Improvement of the purification process…….. 43

4. Glycosylation site confirmation of R27T analogs with additional glycosylation……. 47

5. The analysis of glycosylation……..... 53

6. Protein stability measurement by biophysical analysis ……... 61

7. Maintenance of *in vitro* activity……..... 67

8. Molecular modeling of R27T/IFNAR2 complex…..……..... 69

9. *In vivo* pharmacokinetics study in rats……..... 72

10. *in vitro* activity of PEG-R27T…… 76

11. *in vivo* PEG-R27T pharmacokinetic study in rats…….. 79

V. DISCUSSION……..... 83

VI. CONCLUSION……..... 89

VII. REFERENCE…….. 90

VIII. 국문초록……..... 94

LIST OF TABLES

Table 1. Summary of DMTs……..……. 8

Table 2. Glycosylation site prediction…… 34

Table 3. Volumetric productivity comparison between R27T and Rebif…... 41

Table 4. Comparion of productivity……... 42

Table 5 Sugar composition analysis of R27T and Rebif…… 54

Table 6. LugerSep-N2 peaks with GU values and structures determined from WAX fractions……. 59

Table 7. Secondary structure ratios derived from the ATR-FTIR spectra of rhIFN-β 1a and R27T in solution……. 66

Table 8. Pharmacokinetic parameters for R27T……. 75

Table 9 Pharmacokinetic parameters for PEG-R27T…… 82

LIST OF FIGURES

Figure 1. Epidemiology of multiple sclerosis……. 3

Figure 2. Different types of multiple sclerosis……... 4

Figure 3. Prevalence of the different types of MS..... 5

Figure 4. MS immunopathogenesis and therapeutic targets…… 10

Figure 5. Rational design and engineering of rhIFN-β…….. 13

Figure 6. Construction of a gene encoding a human rhIFN-β glycosylation analogs…… 18

Figure 7. Structural and functional study…….. 33

Figure 8. Construction and testing of rhIFN-β glycosylation analogs…….. 36

Figure 9. Gene amplification with MTX and colony selection……. 39

Figure 10. Growth and R27T production in a batch suspension culture at 34°C 40

Figure 11. Initial purification process and purity of R27T…….. 44

Figure 12. Improvement of the purification process……...…… 45

Figure 13 Product qualification with IEF……... 46

Figure 14. Amino acid sequence of Rebif and R27T ……..... 48

Figure 15. LC/ESI MS/MS of trypsin/Glu-C digests of R27T and Rebif……. 49

Figure 16. MALDI spectra from permethylated R27T samples…….. 55

Figure 17. LugerSep-N2 HILIC-HPLC profiles of R27T WAX fractions…….. 57

Figure 18. DSC thermograms of rhIFN-β 1a and R27T…….. 62

Figure 19. Size distribution of rhIFN-β 1a and R27T……. 65

Figure 20. *In vitro* activity……... 68

Figure 21. Model of the N-glycosylated R27T/IFNAR2 complex……. 71

Figure 22. Mean arterial plasma concentration–time profiles for rhIFN-β……. 74

Figure 23. PEG-R27T *antiviral* activity…….. 77

Figure 24. *In vitro* PEG-R27T activity…… 78

Figure 25. Mean arterial plasma concentration-time profiles……. 81

Figure 26. Innovative drug development strategy……... 89

LIST OF ABBREVIATIONS

rhIFN-β 1a	recombinant human interferon-β1a
MS	multiple sclerosis
DMT	disease modifying treatment
CRAB	Copaxon, Rebif, Avonex, Betaseron
CHO	chinese hamster ovary
DHFR	dihydrofolate reductase
MTX	methotrexate
IEF	isoelectric focusing
RP-HPLC	reversed-phase high-performance liquid chromatography
TFF	tangential flow filtration
CPE	cytopathic effect
PDI	polydispersity index
ΔH	calorimetric enthalpy
ΔH_v	van't Hoff enthalpy
T_m	transition (or melting) temperature
PEG	polyethylene glycol
AUC	total area under the plasma concentration–time curve from time zero to time infinity

$t_{1/2}$	terminal half-life
V_{ss}	apparent volume of distribution at steady-state
CL	time-averaged total body clearance
C_{max}	peak plasma concentration
T_{max}	time to reach at C_{max}
F	extent of absolute bioavailability
ANOVA	analysis of variance

I. INTRODUCTION

1. Multiple sclerosis

Multiple sclerosis (MS) is a chronic neurodegenerative disease that affects the brain and spinal cord, leading to symptoms such as visual field loss, muscle weakness, sensory disturbances, difficulty with coordination and balance, and thinking and memory problems [1-3]. Worldwide, an estimated 2.3 million people were afflicted with MS in 2013 (Figure 1) [4]. Although the distribution of MS is uneven, it is found in every region of the world [4]. The exact cause of MS is still unknown, although complex interactions between infectious, immunologic, genetic, and environmental factors are thought to be involved [5]. MS is characterized by pathologically multifocal areas of demyelination and gliosis within the brain and spinal cord, which contribute to clinical symptoms [5,6]. MS occurs most commonly between the ages of 20 and 50, particularly for women more than men, and its course is variable [3,7]. The clinical course of MS can be categorized into four forms by the progression of symptoms: relapsing-remitting (RR), secondary progressive (SP), progressive-relapsing (PR), and primary progressive (PP) MS (Figure 2) [8]. Approximately 85% of patients start with RRMS. RRMS patients show episodes of exacerbations and remissions during which not all symptoms resolve completely (Figure 3). The majority of RRMS patients are followed by the SP phase, where relapses become more severe while remissions are less complete. A minority of patients (~15%) displays PP characteristics, which features a steady increase in disability with irreversible worsening of clinical signs without attacks

from disease onset.

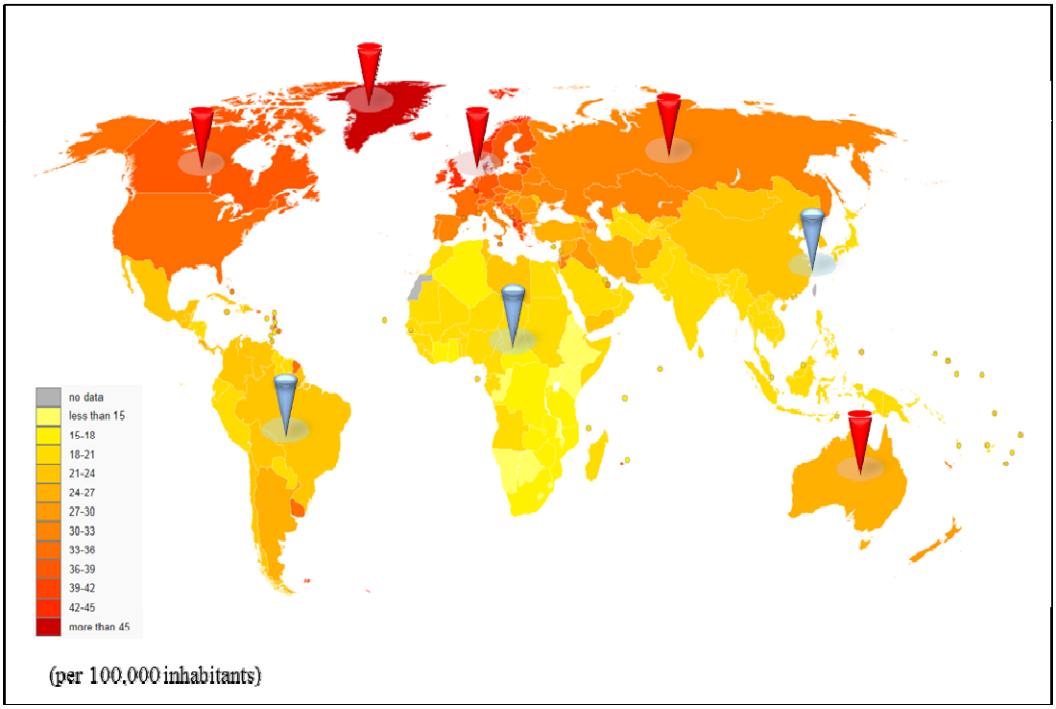

Figure 1. Epidemiology of multiple sclerosis.

Source: Milo R, Kahana E (March 2010). "Multiple sclerosis: geoepidemiology, genetics and the environment". Autoimmun Rev 9 (5): A387–94.

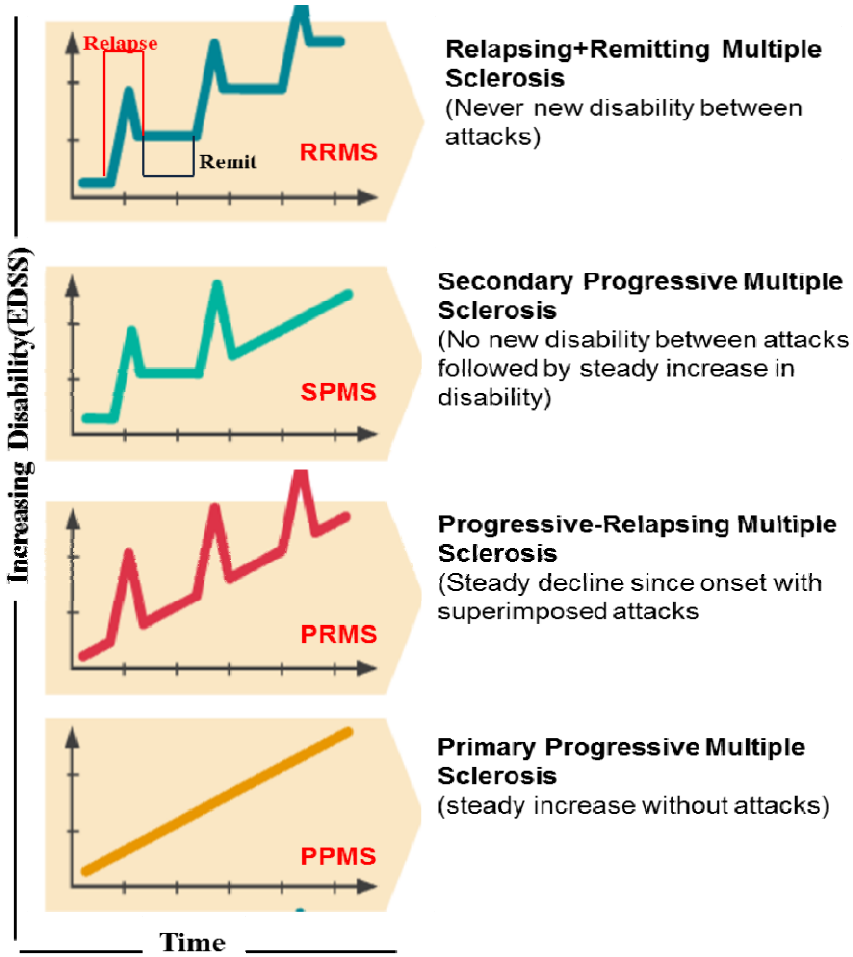

Figure 2. Different types of MS at diagnosis.

Figure 3. Prevalence of the different types of MS.

Source: Editorial in Lancet Neurol. 2012 Oct; 11(10);833.

2. Therapeutics for multiple sclerosis

There are currently a number of disease-modifying treatments (DMTs) approved by the Food and Drug Administration to manage and modify the course of relapsing MS, although there is no cure [9]. Moreover, promising new drugs for MS have been recently licensed or are in late-stage development (Table 1). The therapeutics can be classified into several groups: existing parenteral therapeutics such as rhIFN-β and compaxone, biosuperior versions of rhIFN-β such as PEGylated or deamidated rhIFN-β, oral treatment, and monoclonal antibody therapeutics. The mechanism of action of these DMTs has been explored by Rocio *et al.* [10]. The specific target was based on each step of the MS immunopathogenic cascade, including different aspects of T-cell and B-cell function, mixed targets, and neuroprotective strategies (Figure 4). Among the DMTs, recombinant human interferon-β (rhIFN-β) products like Rebif, Avonex, and Betaseron have been widely used for the first-line treatment for patients and showed long-term safety in recent decades [11,12]. Two very different strategies have been used to generate the three rhIFN-β therapeutics, Avonex (rhIFN-β 1a), Rebif (rhIFN-β 1a), and Betaseron (rhIFN-β 1b). rhIFN-β 1a was expressed in Chinese hamster ovary (CHO) cells to produce a glycosylated form of rhIFN-β that should be structurally indistinguishable from natural IFN-β in its primary sequence and carbohydrate content. rhIFN-β was also expressed as a non-glycosylated protein in *E. coli*. In order to increase yields of biologically active product, *E. coli* IFN-β was engineered to carry a Cys-17 to Ser

mutation, and was later designed as IFN-β 1b because of this change in sequence. The *E. coli* product also contains a Met-1 deletion as a result of the method of production. Although both products appear to have similar biological activities, the *in vitro* potency of commercially available *E. coli* products is lower. While both products have been extensively characterized, they have not been tested side by side in a comparative study and the nature of the structural properties underlying the large differences in potency is unknown.

Table 1. Summary of DMTs

Company	Drug (Parenteral)	Biosuperior Protein for IFN-β (Development Stage)	Clinicl trial	
			(Oral)	(Mab)
Biogen-IDEC	Avonex(IFN-β1a)* Tysabri	• Pegylated IFN-β1a : Patient recruiting for clinical trial III, won FAST TRACK Designation	• Panaclar®(BG12): FDA Approval • Anti-SAM (CDP323): Phase II	• Rituximab* /Ocrelizumab : Failed (with Genentech) • Zenapax® : Ph II (with PDL BioParma)
Merck-Serono	Rebif(IFN-β1a)* Mitoxantrone	• IFNAR2/IFN complex (Patent confirm) • Pegylated IFN-β1a (Published Paper)	• Mylinax®(cladribine) : Approval in Russia (06.2010) and Australia (09.2010) (Movectro®) : Refusal of the marketing authorization in Europe(01, 2011)	
Bayer Healthcatre	Betaseron (IFN-β1b)*		ZK-117137	• Campath®: Ph III (Alemtuzumab, with Genzyme)
Novartis	Extavia(IFN-β1b)*	• Deamidated IFN-β1b (Patent confirm)	• FTY720® (Fingolimod) : Approval in Russia, US FDA, Europe (Gilenya®)	
Sanofi-aventis	Biferonex(IFN-β1a) (with Biopartner) ▪ Refusal in EU		• Teriflunomide ; FDA Approval	

3. Implementation of rhIFN-β therapy for multiple sclerosis

Although rhIFN-β is currently competitive with new oral medicines, providing improved compliance and tolerance, a complete replacement of injection treatments with an oral drug is still uncertain until oral drugs demonstrate long-term safety [12,13]. This is because safety of MS therapeutics is one of the biggest issues, as MS is not a life-threatening disease but a life-long disease since it occurs at an early age [7,12]. On the basis of this, rhIFN-β therapeutics would still account for a sizable portion of the MS therapeutic market for the next several decades. Therefore, a biobetter version of rhIFN-β would address considerable unmet needs in the industrial aspects of the MS therapeutic market including intellectual property issues, biophysical stability and high production cost, and medical aspects, including side effects, short dosing intervals, and route of administration.

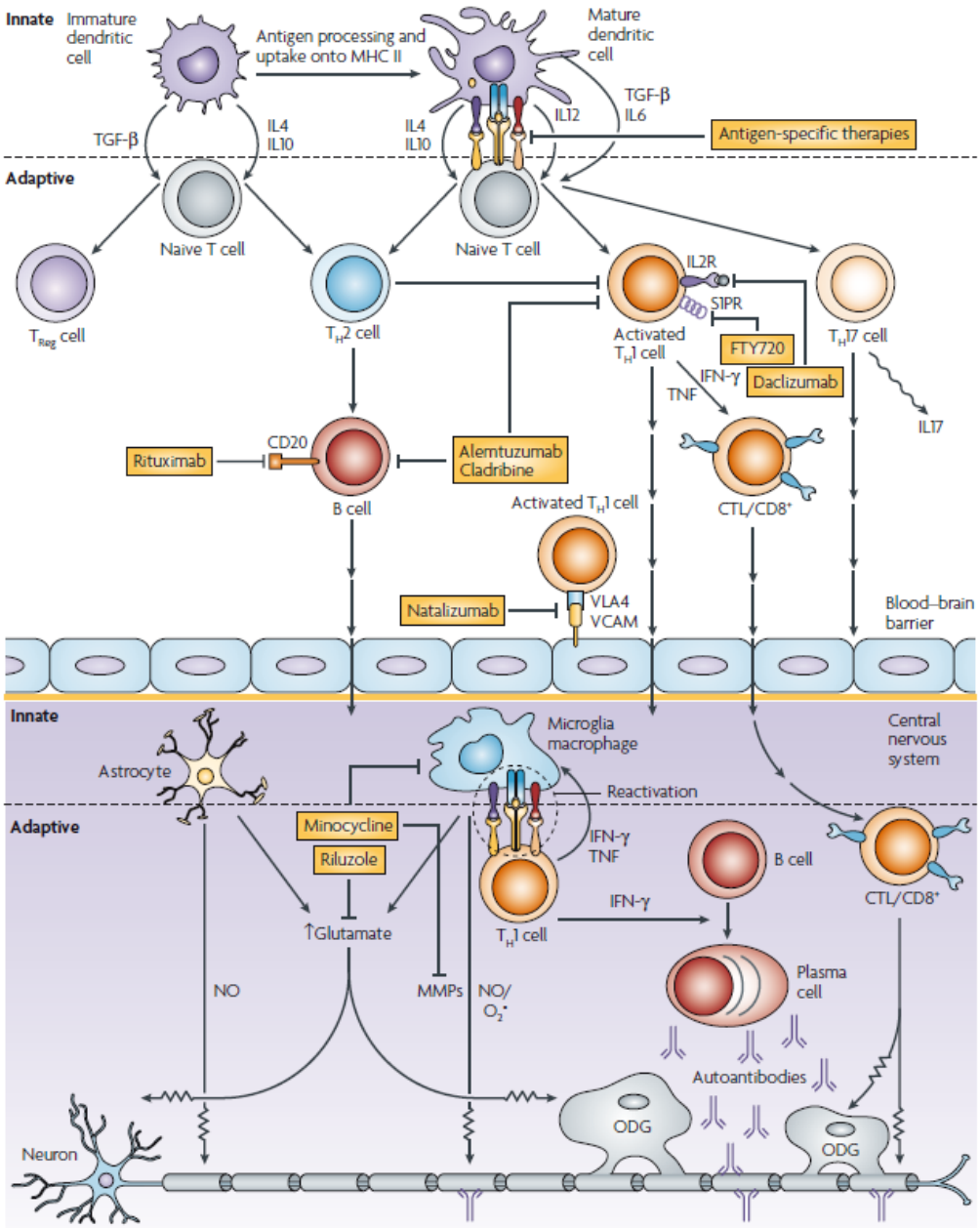

Figure 4. MS immunopathogenesis and therapeutic targets.

Source: Nature Reviews Drug Discovery **7**, 909-925 (November 2008)

4. Rational design and engineering of protein therapeutics

Unlike the synthetic therapeutics, most protein therapeutics have relatively low extent and/or short duration of systemic exposure that may necessitate frequent parenteral administration to achieve efficacy. To overcome these limitations, protein engineering methods including specific mutations, chemical modification and fusion protein have been used for changing biophysical properties of protein therapeutics. So the field of rational design and engineering for protein therapeutics have grown significantly within the pharmaceutical industry. Several engineered protein therapeutics are currently being successfully marketed including Aranesp®, PEGasys®, Neulasta® and so on. These rational modifications can influence the efficacy, stability, specificity, immunogenicity and pharmacokinetics and thus overcome practical constraints such as production costs, intellectual property and patient compliance through changing dosing frequency.

As with other protein drugs, rhIFN-βs have relatively short circulating half-life and low activity that may necessitate frequent parenteral administration to achieve efficacy [14]. To address these issue, glycoengineering and PEGylation is sequencially introduced in rhIFN-β 1a (Figure 5). Historically there is clear evidence for importance of glycosylation in IFN-β therapeutic proteins. There are two kinds of therapeutic rhIFN-β1a (Avonex and Rebif), having 1glycosylation, produced in recombinant CHO cell and IFN-beta 1b (Betaseron), which was produced in *E.Coli* and lack of glycosylation.[15-17] In many reports, IFN-β 1a showed a higher

specific activity and decreased propensity of aggregation than IFN-β 1b [18,19]. Runket *et al.* proved that this remarkable difference was derived from glycosylation in which the glycan plays an important role in protein stability, solubility and immunological differentiation [19]. So, glycosylation engineering would have considered to address industrial production cost. rhIFN-β is a highly hydrophobic protein that has a strong propensity of aggregation and this property affect low protein production yield. Improvement of protein stability and solubility through glycosylation could address cost of goods issue. In addition, introduction of glycosylation consensus sequence through site direct-mutagenesis make it new molecular entity that have only one amino acid change and are added glycosylation to rhIFN-β. To address clinical unmet needs including frequent injection and local skin reaction and immunogenicity, PEGylation was introduced in additionally glycosylated rhIFN-β 1a. Recently, the benefit of PEGylation was clearly seen in rhIFN-β 1a in which N-terminal 20kDa Pegylated IFN-β 1a greatly alters the pharmacokinetic properties of IFN-β 1a, resulting in an increase in systemic exposure following diverse routes [20].

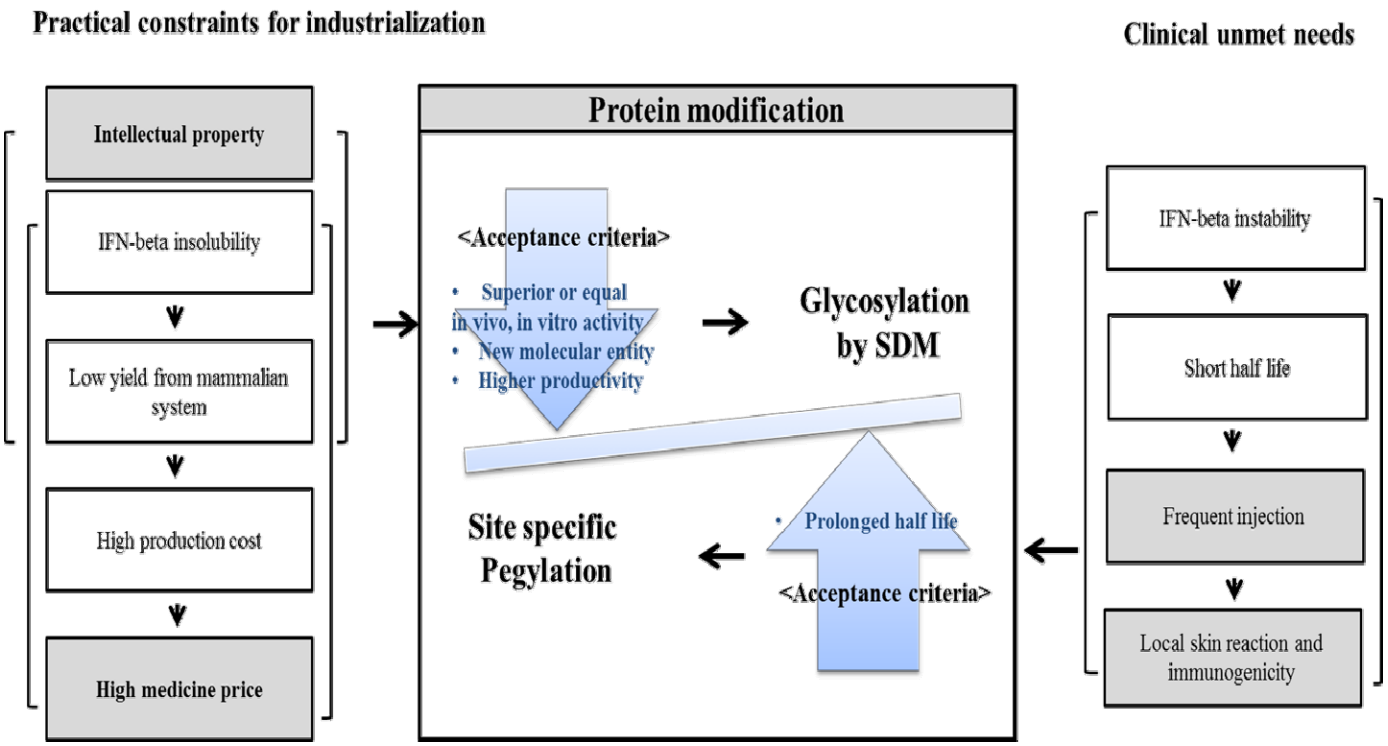

Figure 5. Rational design and engineering of rhIFN-β

II. PURPOSE OF THE STUDY

rhIFN-β 1a is a single glycosylated protein (at N80, 1N) with anti-viral activity. It was approved as a drug for treatment of multiple sclerosis. rhIFN-β is a highly hydrophobic protein that has a strong propensity of aggregation. It was already well known that the aggregation reduce the activity of rhIFN-β and can also affect the low production yield in the mammalian culture systems, which resulted in high price of therapeutics from high cost-of-goods. Additionally, due to relatively low extent and/or short duration of systemic exposure, the frequent injections and related local skin reactions are the most common inconveniences associated with the treatment. To overcome these overall limitations, we sequentially introduced glycosylation and PEGylation on rhIFN-β 1a.

The purpose of this study was to develop a biobetter version of recombinant human rhIFN-β 1a with retained molecular activities, improved biophysical properties, and improved pharmacokinetic properties that could allow the protein to be less aggregative, thus addressing problems such as the production, stability, and subsequent half-life of this protein.

III. MATERIALS AND METHODS

1. Construction of a gene encoding rhIFN-β glycosylation analogs

Glycosylation analogs were constructed by site-directed mutagenesis using PCR with a wild-type human IFN-β gene from a cDNA library from the human fibroblast WI38 cell line (Figure 6). In brief, amino acid substitutions were introduced into the protein in two successive steps by PCR mutagenesis of the gene. In step 1, two reactions (1st PCR and 2nd PCR) were carried out on template wild-type IFN-β cDNA. The 1st PCR used a 5′ (forward) primer and a reverse mutagenic primer. The 2nd PCR used a 3′ (reverse) primer and the forward mutagenic primer. The DNA fragments from the 1st and 2nd PCRs were combined in step 2, in which a third PCR reaction was performed using only the 5′ forward and 3′ reverse primers. The full-length gene was recovered and cloned into the expression vector pMSG. The primers information is as follows: 5′- and 3′- primers for cloning; forward primer sequence: 5′-TTAGCTAGCCACCATGACCAACAAGTG-3′, reverse primer sequence: 5′-GGAGATCTTC A GTTTCGGAGGTAACC-3′; 5′- and 3′- primers for mutagenesis; forward mutagenesis primer sequencing-G143C: 5′-GCAATTGAATGGGACGCTTGAATAT TGCC-3′ reverse mutagenesis primer sequencing -G143C: 5′-GGCAATATTCAAGCGTC CCATTCAATTGC-3′. The sequences of all constructs were verified by DNA sequencing.

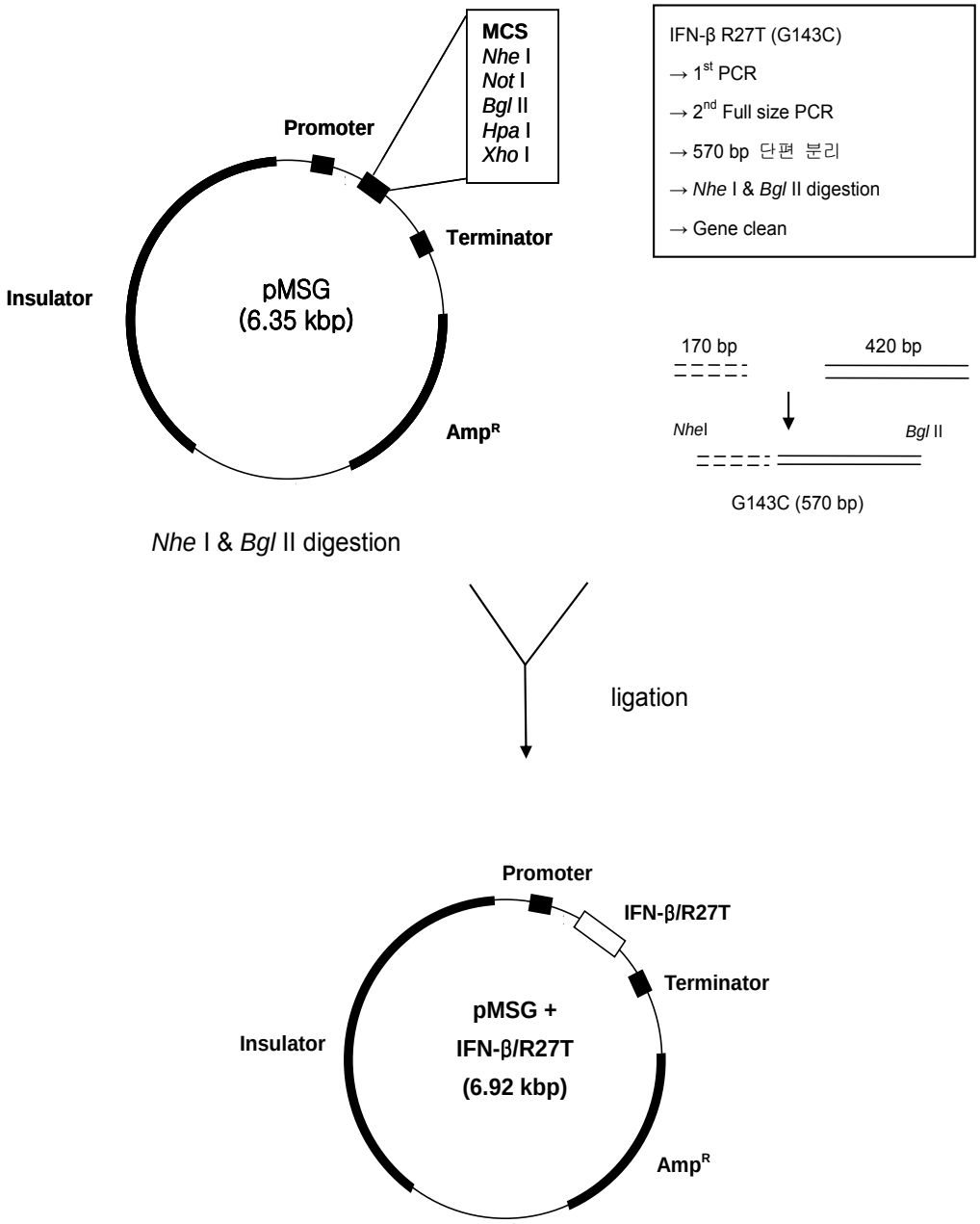

Figure 6. Construction of a gene encoding human rIFN-β glycosylation analogs.

2. Expression of rhIFN-β construct in mammalian cells

rhIFN-β glycosylation analogs were transiently transfected into COS cells (ATCC No. CRL-1650) using the liposome method. After serum-free DMEM was added to the lipofectamine-DNA complex, the mixture was gently placed on the COS cells cultured in a plate, and the plate was incubated in a 37°C, 5% CO_2 incubator for 6 h to allow the transfection to occur. The stable transfection into CHO cells was accomplished with a dihydrofolate reductase selection system and selected MTX resistance clones were grown in MTX selective medium. Expression of each rhIFN-β muteins in mammalian cell lines was confirmed by western blot analysis.

3. Purification and characterization of rhIFN-β mutants

Filtered crude harvests were purified by affinity chromatography, ion exchange chromatography, reverse-phase liquid chromatography, and size-exclusion chromatography. First, for purification of rhIFN-β muteins, culture fluid containing rhIFN-β mutant proteins was applied to a column of blue Sepharose 6FF (GE Healthcare, Buckinghamshire, UK) at 80 mL/min and washed with 20 mM sodium phosphate monobasic dihydrate. The bound protein was eluted with 35% propylene glycol in a phosphate buffer and directly loaded onto CM Sepharose FF (GE Healthcare). After application, the column washed with 20 mM phosphate buffer, pH 2.9, and rhIFN-β was eluted with phosphate-buffered 145 mM NaCl, pH 7.0. The

eluted sample was applied to a C4 RP-HPLC column (VYDAC, CA, USA) at 15 mL/min and washed with 30% acetonitrile and 0.1% trifluoroacetic acid. R27T was eluted with a linear gradient. The purified R27T was concentrated and diafiltrated using a 10-kDa cut-off membrane in the Millipore Lab scale TFF system (Millipore, MS, USA). Finally, gel filtration chromatography was performed using a Sephacryl 100HR column at 2.5 mL/min.

4. Analysis of expressed proteins

Purified rhIFN-β mutant proteins were assessed by SDS-PAGE and western blot analysis using anti-hIFN-β (R&D systems, Minneapolis, MN, USA) as the primary antibody. To confirm the presence of glycosylation, 1 mg/mL R27T in 20 mM sodium phosphate buffer, pH 7.5, was treated with PNGase F (Sigma, St. Louis, MO, USA) at 37°C. Samples were taken at each time point over 1 h. Deglycosylation was monitored by SDS-PAGE. IEF (Invitrogen, CA, USA) was conducted at pH 3~10 for the analysis of the pH at the isoelectropoint (pI) according to the manufacturer's instructions. The concentration of R27T in media samples was quantified using an rhIFN-β ELISA kit (IBL, Hamburg, Germany) according to the manufacturer's instructions.

5. Glycosylation site confirmation

Site-specific glycosylation analysis of R27T was carried out using RP-HPLC coupled with electrospray ionization tandem mass spectrometry (LC/ESI MS/MS). R27T was reduced and then digested with trypsin/Glu-C. The glycopeptide ions were extracted and confirmed by the presence of carbohydrate-specific fragment ions, such as *m/z* 204 (HexNAc) and 366 (HexHexNAc), in the product ion spectra. To identify exact site of glycosylation, PNGase F was then used to remove N-linked glycans from the trypsin/Glu-C glycopeptides and convert Asn into Asp. Deglycosylated peptides were sequenced by LC/MS/MS.

6. Monosaccharide and sialic acid composition analysis

A Dionex HPAEC system (Dionex, CA, USA) was used to analyze the monosaccharide and sialic acid composition of the proteins. An AminoTrap column (4 × 50 mm, Dionex) and a Carbopac PA10 analytical column (4.6 × 250 mm, Dionex) were used at 1 mL/min and 30°C. NaOH (100 mM) and NaOAc (1 M) were used to analyze acidic sugars. NaOH (18 mM) followed by a linear 200 mM NaOAc gradient was used to analyze all monosaccharides, including neutral, amino, and acidic sugars. The waveform of PAD was the Dionex default program for carbohydrates. The injection volume was set to 10 μL. The retention time of each monosaccharide standard in the mixtures with different methods was confirmed by the analysis of each monosaccharide individually.

7. Oligosaccharide profiling

Aliquots (1 μL) of the unlabeled portion of the N-glycan released from the R27T sample were taken for permethylation analysis along with negative and positive controls, buffer, water, and Futuin. Unlabeled glycan samples were permethylated using methyl iodide in a DMSO/NaOH suspension. Permethylated glycans were obtained from the solution by chloroform extraction and samples were run on a Shimadzu-Biotech Resonance MALDI mass spectrometer using DHB as the matrix (10 mg/mL, 2,5-dihydroxybenzoic acid in acetonitrile). R27T was reduced and alkylated and then set in an SDS-PAGE gel block. Samples were set into a gel block and washed before overnight incubation with PNGase F. The released glycans were eluted, converted to aldoses, filtered, and then dried. The cleaned glycans were resuspended in 20 μL water. 2-AB labeling was conducted using GlycoProfile Labeling kits (LudgerTag 2-AB). Anion exchange chromatography of 2-AB-labeled glycan was performed using a LudgerSep-C3 column 7.5 × 75 mm; the column temperature was set at 35°C and 25-μL aliquots of the sample were injected. A gradient of 100% A for 5 min followed by 100%~96% A over 5 min~21 min, then 96%~75% A over 21 min~61 min, then 75%~60% A over 61 min~72 min, then 60% A for 72 min~75 min at a flow rate of 0.4 mL/min, before washing with 100% A for 76 min~90 min at 0.8 mL/min. Solvent A was 20% acetonitrile in water and Solvent B was 500 mM ammonium acetate with 20% acetonitrile. The HPLC system consisted of a Waters Alliance 2795 separation unit

with a Waters 2475 fluorescence detector controlled by Empower2.

8. Exoglycosidase digestion

2-AB-labeled glycans were dried and digested with various exoglycosidases. The R27T sample was incubated overnight at 37°C with exoglycosidases in 50 mM sodium acetate, pH 5.5. Enzymes were removed using a protein binding membrane before analysis by HPLC.

9. Protein stability measurement by biophysical analysis

Dynamic light scattering (DSC) measurements were performed using a VP-DSC Microcalorimeter (MicroCal, MA, USA). Calorimetric scans were carried out between 25 and 120°C with a scan rate of 1°C/min. To determine the thermal properties of proteins in solution, heat capacity curves were generated and evaluated using MicroCal Origin 7.0 software. Hydrodynamic size was investigated using a Zetasizer Nano ZS90 (Malvern Instruments, Baden-Württemberg, Germany). The temperature in the Zetasizer chamber was equilibrated to 10°C. Each sample was measured in a disposable sizing cuvette (Sarstedt, Germany). Hydrodynamic size and polydispersity index (PDI) were calculated from the auto-correlation function using Zetasizer software, version 6.32 (Malvern Instruments). Atteuated total reflectance Fourier Transform Infrared (ATR-FTIR) spectra (4000–600 cm^{-1}) were

collected at 4 cm^{-1} resolution using a Nicolet 6700 spectrophotometer (ThermoFisher Scientific, MA, USA) with a golden gate accessory (diamond crystal). The α-helix, β-sheet, β-turn, and random coil contents of the proteins were estimated from the amide I region of the ATR-FTIR spectra. Peaks of the amide I region were first treated by Fourier self-deconvolution and then curve-fitted using the Gauss and Lorentz formula with OMNIC Peak Resolve software (ThermoFisher Scientific). The area corresponding to each secondary structure was calculated accordingly and expressed as a percentage of the sum of areas. To measure kinetic thermostability, rhIFN-β 1a and R27T were incubated for 96 h at 37°C and decay curves were generated for each protein. Detectable rhIFN-β was quantified using the cytopathic effect (CPE) assay at each sampling time.

10. Determination of antiviral activity

Antiviral activity was measured for each mutein of rhIFN-β 1a, R27T, and PEG-R27T with Rebif as a standard. A549 cells were cultured in MEM medium supplemented with 10% FBS, 1 mM MEM nonessential amino acid, and 1 mM sodium pyruvate. On the day of analysis, cells were laid in fresh medium and the density of the cells was adjusted to 300,000 cells/mL. Samples in the experimental group and control group were diluted. Dilutions were carried out in a 96-well microtiter plate after delivering 100 μL/well. All samples were tested in quintuplicate. Control wells contained only 100 μL of medium (without IFN-β).

After delivering 100 μL of cells per each well, the plate was incubated in 5% CO_2 at 37°C for 22 h. After removing the medium from the plate, 100 μL of EMCV (1000TCID50/mL) was added to each well except for the cell control line. After incubation of plate in 5% CO_2 at 37°C for 22 h, the plate was removed and dyed with crystal violet. After removing the dye, 100 μL of 2-methoxyethanol was added and dyeing solution was extracted. Antiviral activity was measured at the absorbance of 570 nm.

11. Anti-proliferative activity

The anti-proliferation effect of rhIFN-β 1a muteins and PEG-R27T was measured with the control sample, Rebif, using Daudi cells. Daudi cells were cultured in RPMI 1640 medium supplemented with 2 mM of glutamine and 10% FBS. rhIFN-β in experimental group and control group were diluted using RPMI 1640 medium containing 10% FBS. Dilution was carried out in a 96-well microtiter plate after delivering 100 μL/well. All samples were tested in duplicate. Cells were distributed at a concentration of 10,000 cell/well in a 96-well plate and incubated in 5% CO_2 at 37°C for 48 hours. Measurement of cell proliferation was then performed using an EZ-Cytox Cell viability assay kit following the manufacturer's protocol.

12. Immunomodulatory effect

The immunoregulatory function of wild-type rhIFN-β, derived muteins, and PEG-R27T were measured by the activation of MHC Class I in A549 cells. A549 cells were cultured in DMEM medium containing 10% FBS and 2 mM glutamine. After dilution, cells, were delivered to the medium containing diluted rhIFN-β at a concentration of 2×10^5 cell/mL. The cells were then incubated in 5% CO_2 at 37°C for 48 h. After treating the cells with 0.25% trypsin EDTA, they were collected by centrifugation. Cells were diluted to a concentration of 1×10^7 cell/mL with FACS buffer and the expression of MHC class I was measured by FACS analysis. Anti-human HLA-ABC antibody coupled with biotin and streptavidin coupled with fluorescent dye were used for detection. All samples were tested in duplicate.

13. Molecular modeling of R27T/IFNAR2 complex

The molecular models of the glycosylated rhIFN-β 1a were built from the crystal structure of wild-type rhIFN-β 1a (PDB ID:1AU1) [21]. Mutation of arginine to threonine at the 27th residue and N-linked glycosylation of 1AU1 were performed using UCSF Chimera [22,23] and GLYCAM [24-26]. Due to the high sequence identity (approx. 30%) between IFN-β 1a and IFN-α-2a, initial IFN-β 1a/IFNAR2 complex structures were generated using structural alignment with the model of IFN-α-2a/IFNAR2, which was previously determined using the NMR-based docking method (PDB ID:2HYM) [27]. For N-glycosylation of the initial complex structure, a bulky oligosaccharide was used with one of the major peak fractions from the

oligosaccharide mixture through HILIC profile of R27T weak anion exchange (WAX) fractions. The oligosaccharide was built using Carbohydrate Builder (Woods Group. 2005-2013, GLYCAM Web. Complex Carbohydrate Research Center, University of Georgia, Athens, GA., http://www.glycam.com) and was attached to the N-glycosylation site of the wild-type IFN-β 1a/IFNAR2 structure. The final structures were minimized at amber force field (AMBER99SB) [28]. During minimization, Amber parameters were used for standard residues, and an Antechamber module was used to make parameters to non-standard residues. One hundred steps of steepest minimization were then performed to relieve unfavorable clashed, followed by 100 steps of conjugate gradient minimization. The size of the steepest descent and conjugate gradient minimization was 0.02 Å. Molecular visualization was performed using UCSF Chimera and Pymol (The PyMOL Molecular Graphics System, Version 1.2r3pre, Schrödinger, LLC).

14. PEGylation of R27T

PEGylation of R27T was carried out by reacting R27T (2.0 mg/mL) with 20 kDa or 40 kDa mPEG-aldehydes (mPEG-ALD-20K or mPEG-ALD-40K) in 20 mM phosphate buffer, pH 5.5, containing 5 mM sodium cyanoborohydride. The reaction was performed with a molar ratio of 1:5 (protein:ALD-mPEG) at 4ºC overnight.

15. Purification of PEG-R27T

To remove unreacted PEG, the reaction mixture was directly loaded onto Vivapure ion-exchange spin columns with a sulfonic acid ligand (Sartorius Stedim Biotech GmbH, Goettingen, Germany) that had been equilibrated with 0.1 M phosphate buffer (pH 5.5). The spin column was washed with the same equilibrium buffer and then bound proteins were eluted with 0.1 M phosphate buffer containing 1 M NaCl (pH 5.5). The eluted fraction was immediately loaded onto a Superose 6 HR 10/30 size-exclusion column equilibrated with 20 mM phosphate buffer containing 150 mM NaCl (pH 5.5) as the mobile phase. A flow rate of 0.5 mL/min was used and UV absorbance was monitored at 215 nm. The mono-PEGylated R27T fraction was pooled, concentrated with Centricon YM 3 (Millipore), and filter-sterilized through a 0.2-μm membrane filter. The concentration was determined by the absorbance at 280 nm based on the absorbance of unmodified R27T, since mPEG-ALD does not have UV absorbance. PEGylated R27T was stored at -20ºC until use.

16. *In vivo* pharmacokinetic analysis in rats

Male Sprague–Dawley rats (weighing 200−250 g), 6−8 weeks of age, were purchased from Orient Bio, Inc. (Seongnam, South Korea). Protocols for the animal studies were approved by the Institutional Animal Care and Use Committee of the

Seoul National University (Seoul, South Korea, SNU-200909-33). The femoral artery and vein were cannulated with a polyethylene tube (PE-50; Clay Adams, Parsippany, NJ, USA) under light ketamine anesthetization (50 mg/kg). rhIFN-β substances (R27T, mixture R27T, PEG-20K, PEG-40K, and Rebif) were bolus-injected intravenously (via the femoral vein; IV), subcutaneously (at the abdomen; SC), or intramuscularly (at the leg; IM) at a dose of 1 MIU/kg to rats (total injection volume of approximately 0.3 mL). An approximately 120-μL aliquot of blood was collected via the femoral artery at 0 (to serve as a control), 1, 5, 15, 30, 60, 120, 240, 480, 720, and 1,440 min after IV administration and at 0 (to serve as a control), 15, 30, 45, 60, 120, 180, 240, 360, 480, 720, and 1,440 min after SC and IM administration. An approximately 0.3-mL aliquot of the heparinized 0.9% NaCl-injectable solution (20 IU/mL) was used to flush each cannula immediately after each blood sampling to prevent blood clotting. Blood samples were centrifuged immediately, and a 50-μL aliquot of each plasma sample was stored at −80ºC (Revco ULT 1490 D-N-S; Western Mednics, Asheville, NC) until CPE analysis. Standard methods were used to calculate the following pharmacokinetic parameters by a non-compartmental analysis (WinNonlin, standard version 3.1; Pharsight, Mountain View, CA) [29,30].

Standard methods were used to calculate the following pharmacokinetic parameters using a non-compartmental analysis (WinNonlin, standard version 3.1): the total area under the plasma concentration–time curve from time zero to time infinity (AUC), terminal half-life ($t_{1/2}$), time-averaged total body clearance (CL), and

apparent volume of distribution at a steady state (V_{ss}) [31]. The extent of absolute bioavailability (F) was calculated by dividing the AUC after SC or IM administration by the AUC after IV administration. The peak concentration (C_{max}) and time to reach C_{max} (T_{max}) were directly read from the experimental data.

17. Statistical analysis

A p-value less than 0.05 was considered to be statistically significant using Duncan's multiple range test of the Statistical Package for the Social Sciences (SPSS) posteriori analysis of variance (ANOVA) among three means for the unpaired data. All results are expressed as the mean ± standard deviation, except the median (ranges) for T_{max}.

IV. RESULTS

1. Construction of rhIFN-β glycosylation analogs, R27T

Five helical regions, which consist of amino acid residues 2–22 (A), 51–71 (B), 80–107 (C), 112–136 (D), and 139–162 (E), were excluded for an additional N-glycosylation site that best maintain the structural and functional properties of the protein (Figure 7). A few sites, including Arg 27, Asp 39, Gln 72, Asp 73, Ser 74, Ser 75, Asp 110, and Glu 137, were screened for the introduction of a consensus sequence (Asn-X-Ser/Thr, where X is any amino acid except proline) for additional N-glycosylation, in which each of the sites was analyzed by the NetNGlyc program in CBS prediction servers (Table 2).

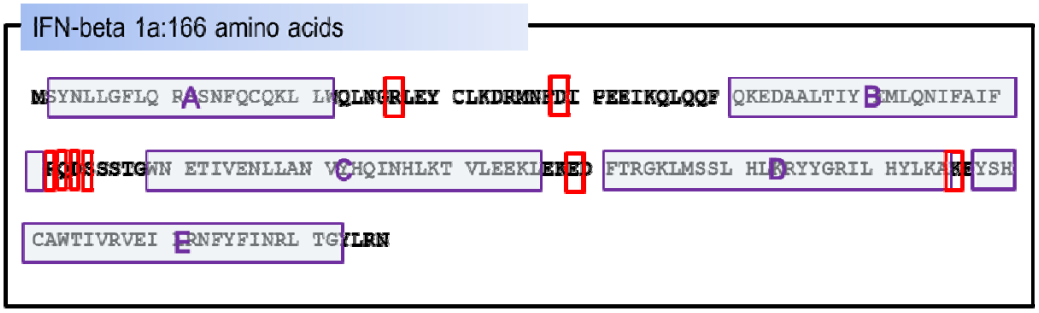

- Non-helical regions: less likely to be critical for structure and stability

→ Arg27, Asp39, Gln72, Asp73, Ser74, Ser75, Asp110 and Glu137

- Most Flexible overhand AB loop and the highest mobility CD loop

→Arg27, Asp39, Asp110

Figure 7. Structural and functional study.

Table 2. Glycosylation site prediction

#	mutation			substitution site			80th amino acid(80N)			DNA sequence substitution
	A.A change	N site	4 aa	potential	agree	Result	potential	agree	Result	
Native			NETI				0.5903	7/9	+	
1	**R27T**	25N	NGTL	0.7229	9/9	++	0.5902	7/9	+	AGG -> ACG
2	**R27S**	25N	NGSL	0.6654	9/9	++	0.5902	7/9	+	
3	**D39T**	37N	NFTI	0.6983	9/9	++	0.5903	7/9	+	
4	**D39S**	37N	NFSI	0.6388	9/9	++	0.5902	7/9	+	
5	**Q72N**	72N	NDSS	0.5261	5/9	+	0.5943	7/9	+	
6	**D73N**	73N	NSSS	0.6810	9/9	++	0.5807	7/9	+	
7	**S74N**	74N	NSST	0.3662	7/9	-	0.5459	6/9	+	
8	**S75N**	75N	NSTG	0.5256	8/9	+	0.5724	7/9	+	
9	**D110N**	110N	NFTR	0.4982	2/9	-	0.5902	7/9	+	
10	**E137N**	137N	NYSH	0.5313	4/9	+	0.5902	7/9	+	
11	"+GNITVNITV"	168N	NITV	0.7233	9/9	++	0.5948	7/9	+	GCTAATATCACTGTC
		172N	NITV	0.6587	9/9	++				AATATCACTGTC

We used the analyzed data to target the most flexible overhand AB loop and the highest mobility CD loop remaining Arg27, Asp39, and Asp110 to minimize structural modification by bulky residues derived from additional glycosylation (Figure 8A). The Arg27 site of IFN-β was chosen as the most promising site, which had the highest substitution potential score by the NetNGlyc program, and Asp110 was chosen as a negative control, respectively. In addition, the hyper-glycosylated rhIFN-β model was created by the extension of sequence "ANITVNITV, (NITV)2" into the C-terminal domain. R27T and the R27T-(NITV)2 mutant showed a clear increase in molecular weights by 26 and 30 kDa, respectively, by western blot analysis. It was confirmed by SDS-PAGE after rhIFN-β purification that while there was no change in the D110N analog, compared to the native rhIFN-β (Figure 8B, 8C). Treatment with PNGase, which catalyzes the release of N-linked oligosaccharides, resulted in the appearance of three bands of 26, 22, and 18 kDa in the R27T sample (Figure 8D). The upper and middle bands include two and one glycosylation, respectively, whereas the lower band contains only the peptide. Thus, the incremental increase in the molecular weight was attributed to additional glycosylation. The negative charge was increased in R27T and R27T-(NITV)2, which showed pI values of 5.3~6.4 and 4.6~6.4, respectively, compared to pI 7~8 for native rhIFN-β (Figure 8E). R27T, having one additional glycosylation at the 25th amino acid, was selected as a lead protein because the amino acid change required for additional glycosylation was minimal, which could be more meaningful than R27T-(NITV)2, in regards to immunogenicity.

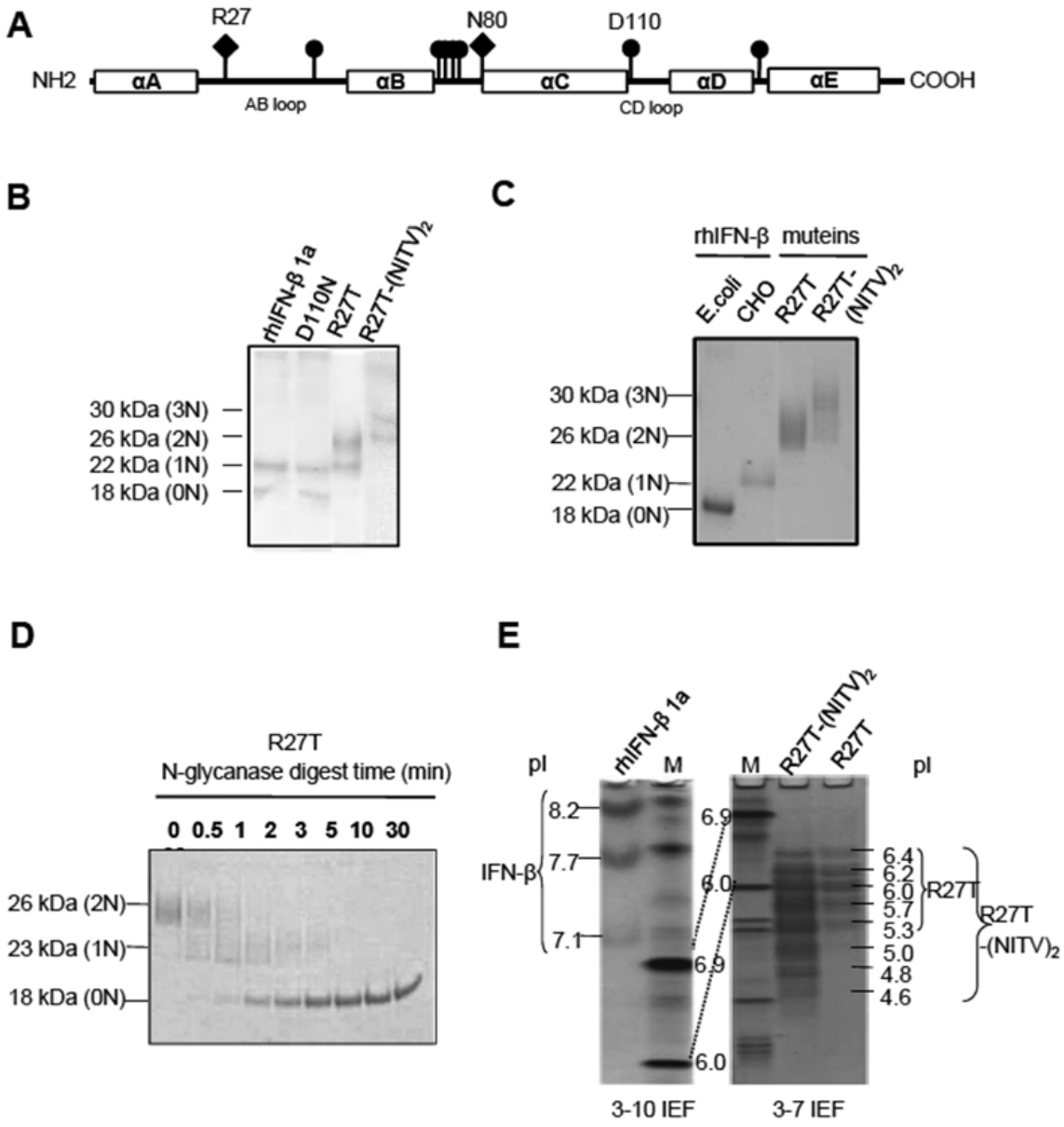
A
R27
N80
D110
NH2
αA
αB
αC
αD
αE
COOH
AB loop
CD loop
B
rhIFN-β 1a
D110N
R27T
R27T-(NITV)2
30 kDa (3N)
26 kDa (2N)
22 kDa (1N)
18 kDa (0N)
C
rhIFN-β
muteins
E.coli
CHO
R27T
R27T-(NITV)2
30 kDa (3N)
26 kDa (2N)
22 kDa (1N)
18 kDa (0N)
D
R27T
N-glycanase digest time (min)
0 0.5 1 2 3 5 10 30
26 kDa (2N)
23 kDa (1N)
18 kDa (0N)
E
pI
rhIFN-β 1a
M
M
R27T-(NITV)2
R27T
pI
8.2
7.7
7.1
IFN-β
6.9
6.0
6.9
6.0
6.4
6.2
6.0
5.7
5.3
5.0
4.8
4.6
R27T
R27T
-(NITV)2
3-10 IEF
3-7 IEF

Figure 8. Construction and testing of rhIFN-β glycosylation analogs. (A) A schematic view of the rhIFN-β protein. Boxes represent the locations of the five α-helices. Each vertical line represents a position with the potential for an additional N-linked glycosylation site, as predicted by NetNGlyc. Introduced N-linked glycosylation consensus sites are represented by diamonds (◆). (B) Purified samples were separated by SDS-PAGE. (C) Western blot analysis. (D) Analogs were subjected to N-glycanase digestion for the indicated times. (E) IEF analysis was performed over a pH range of 3~10.

2. Development of cell line and its productivity

The R27T analog was expressed stably in an attached CHO cell line and amplified with MTX. Production of R27T was determined by ELISA (Figure 9). Selected colonies, 19-20 and 19-23, were adapted to serum-free media conditions. The batch culture for protein production was maintained at 34°C for 6 days (Figure 10). During this time, cell density and viability were examined daily and the amount of R27T in the medium was measured using an IBL ELISA kit in the three batches (Table 3). The maximum viable cell density obtained was 2~4 × 10^6 cells/mL, the viability was more than 90% of the maximum cell density, and the R27T accumulated to 9~16 MIU/mL in the medium without any optimal media additives over the 6 days of culture.

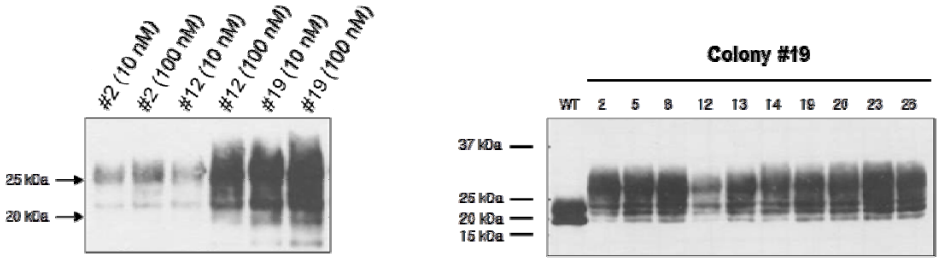

Cell line	Cell Number ($1x10^5$cells/well)		Expression rate		
	Initial	Final	rhIFN-β (MIU/mL)	MIU/10^9 cells/day	μg/10^9 cells/day
19-20 (100 nM)	2.64	6.78	1.026	2.178	10.9
19-23 (100 nM)	1.8	6.96	1.402	3.201	16.0

*rhIFN-β conc./((Initial+final)/2) cell number/2days

Figure 9. Gene amplification with MTX and colony selection.

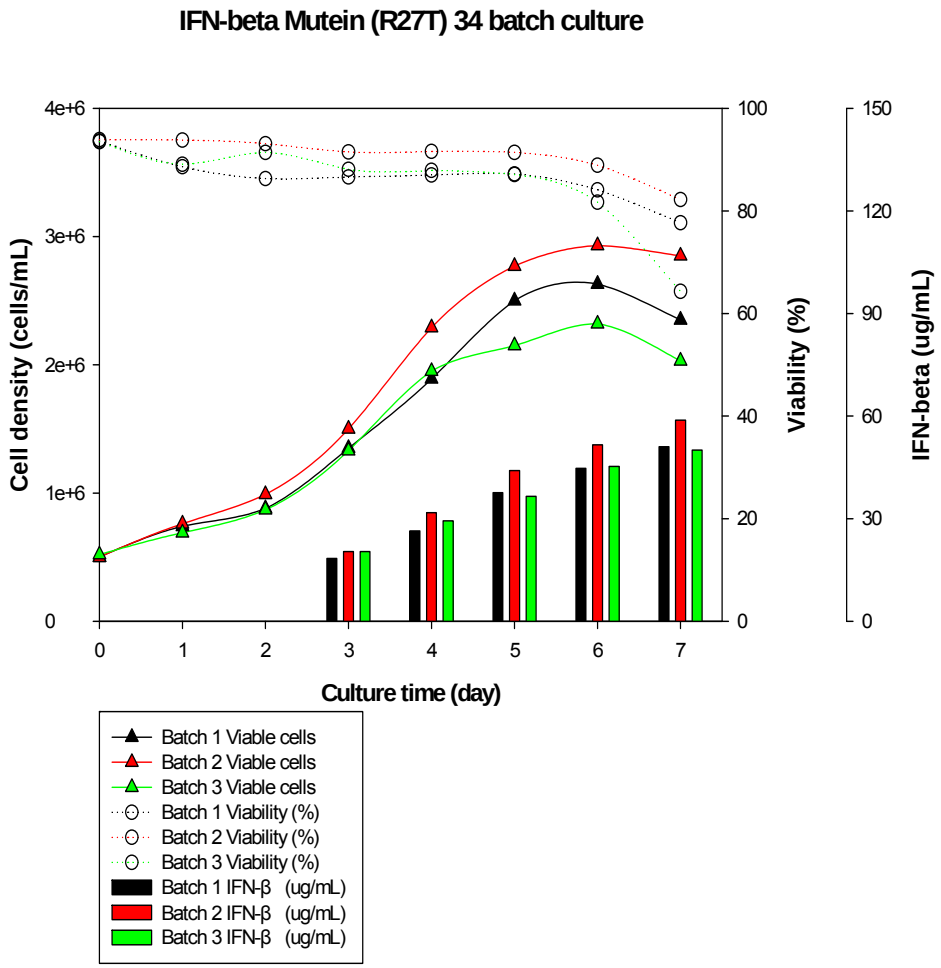

Figure 10. Growth and R27T production in a batch suspension culture at 34°C.

Table 3. Volumetric productivity comparison between R27T and Rebif

1.R27T: volumetric productivity at different phases of the culture

Culture scale	Temperature (° C)	Max. Cell Density (X106cells/mL)	Total Volumetric Production (X106 IU/mL), 300MIU/mg
200mL Spinner flask	37-->34 shift	2	15→50ug/mL
7.5L Bioreactor	37-->34 shift	4	16→53ug/mL
30L Bioreactor	37-->34 shift	4	9→30ug/mL

2. Rebif

Cell culture controls parameters

Three parameters have been selected as indicative of the cell culture conditions in the bioreactors.

Indicative parameter (bioreactor sampling)	Acceptance criteria
Cell count (not adherent cells)	≤ 1 X 10^6 cells/ml
IFN-β-1a titer by ELISA	150,000~550,000 IU IFN-β-1a/ml (0.15~0.55MIU/mL)→0.5ug/mL~1.9ug/mL(288MIU/mg 기준)
Cell viability	≥ 80%

$$\frac{\text{R27T}}{\text{Rebif}} = \frac{(50+53+30)/3}{1.9} = 23$$ → 23 times R27T production improvement

Table 4. Comparison of productivity

Culture condition	Temperature(℃)	Additives	Culture period(day)	Max cell density (cells/mL)	Specific Productivity Qp (β-IFN units/cell/day)	Total volumetric production (x 10^6 units/ml) (x 10^6 units/mL, Non-denatured)	(x 10^6 units/mL, denatured)	End culture viability(%)	Reference
Batch(Spinner Flask)	37		7	3.00E+06		1	3.7		Maureen Spearman et al, Biotech. Prog. 2005, 21,31-39
Batch, Microcarrier(Cytopore 1 1mg/ml)	37		7	1.50E+06		5	14		
Batch, Microcarrier(Cytopore 2 1mg/ml)	37		7	1.50E+06		5	8		
Batch(Bioreactor 2L)	37		7	3.80E+06		1.5	7.5		
Batch, Microcarrier(Cytopore 1 1mg/ml)	37		7	3.00E+06		5.8	10		
Batch(Bioreactor 2L)	37		7	4.20E+06*	0.95	1.3	14		J. Rodriguez et al, Biotechnol. Prog. 2005,21,22-30
Batch(Bioreactor 2L)	37	2% Glycerol	7	3.20E+06*	0.85	6.7	9.6		
Batch(Bioreactor 2L)	37	1% DMSO	7	2.00E+06*	2	2.5	12.8	85%	
Batch(Bioreactor 2L)	37	1mM NaBu	5	1.30E+06*	3.5	1.5	8.9		
Batch(Spinner Flask)	37		8	3.50E+06		0.5	1.5		
Batch(Spinner Flask)	30		14	7.50E+05		3.3	3.6	>90%	
Batch(Spinner Flask)	37 → 30 shift		12	1.80E+06		4.2	9		
Batch(Bioreactor 2L)	37		7	3.20E+06		0.4	3		Maureen Spearman et al, Cell Technology for Cell Products,2007, 71~85
Batch(Bioreactor 2L)	37	1mM NaBu	5	1.50E+06		2	7.5		
Batch(Bioreactor 2L)	37	40mM NaCl	7	2.30E+06		2.1	5.5		
Batch, Microcarrier (Cytopore 1 1mg/mL)	37		7	2.50E+06		2.2	4		
Batch(Spinner Flask)	37		6	3.45E+06		0.96	1.7		
Batch(Spinner Flask)	37 → 30 shift		6	1.80E+06		4.4	5.6	>90%	
Batch(Spinner Flask)	30		10	6.90E+05		1.5	2.35		
Batch(Spinner Flask)	37	2% Glycerol	6	2.05E+06		1.7	4.5		
Batch(Spinner Flask)**	32		10	1.6E+05		2.2		93%	Kelvin Sunley et al., Biotechnol. Prog. 2008, 24,898-906
Batch(Spinner Flask)**	37 → 32 shift		10	6.9E+05		2.4		98%	
Batch(Spinner Flask)**	37		6	4.1E+06	0.341	4.24			
Batch, Microcarrier(Cytopore 2 1mg/ml)**	37		6	2.5E+06	0.954	5.19			
Batch(Spinner Flask)**	32		12	1.7E+05	0.784	1.32			
Batch, Microcarrier(Cytopore 2 1mg/ml)**	32		12	8.2E+05	0.847	3.27			
Batch(Spinner Flask)***	37		10	1.1E+06		5.7		93%	
Batch(Spinner Flask)***	37 → 32 shift		10	2.5E+06		7.1		88%	
Batch(Spinner Flask)***	32		12	2.5E+05	0.233	0.73			
Batch, Microcarrier(Cytopore 2 1mg/ml)***	32		12	5.0E+06	0.92	10.1			
Batch(Bioreactor 2L)	37		0-3	1.39E+06	0.75	0.9	1.5		J. Rodriguez et al, Journal of Biotechnology 2010,150,120
Batch(Bioreactor 2L)	32		3-8	2.55E+06	1.2	12.4	17.4		
Perfusion(Bioreactor 2L)	32		8-16	3.70E+06	2.6	9.3	9.9	>95%	

Atmosphere : 10% CO_2 ** Low Temperature Non-adopted

* Final Cell Yield(cells/mL) *** Low Temperature adopted

3. Improvement of the purification process

The purification process was designed to purify R27T to a purity greater than 99%. Initial purification of the active ingredient started with dye affinity chromatography on Blue Sepharose 6FF, which was the major purification step. To obtain highly purified R27T, three main types of column-based protein separations were chosen. Ion-exchange chromatography on CM-Sepharose FF, reverse-phase HPLC, and gel filtration were utilized sequentially. However, the purity of purified R27T was less than 95% (Figure 11). There was no purification step for separation between single- and double-glycosylated isoforms. Therefore, to purify the double-glycosylated protein from single-glycosylated R27T, the three column-based steps were replaced with a single column step using Q-Sepharose FF (Figure 12). Q-Sepharose FF with pH control in the elution buffer resulted in the purification of double-glycosylated R27T to an extent greater than 99% (Figure 13).

.

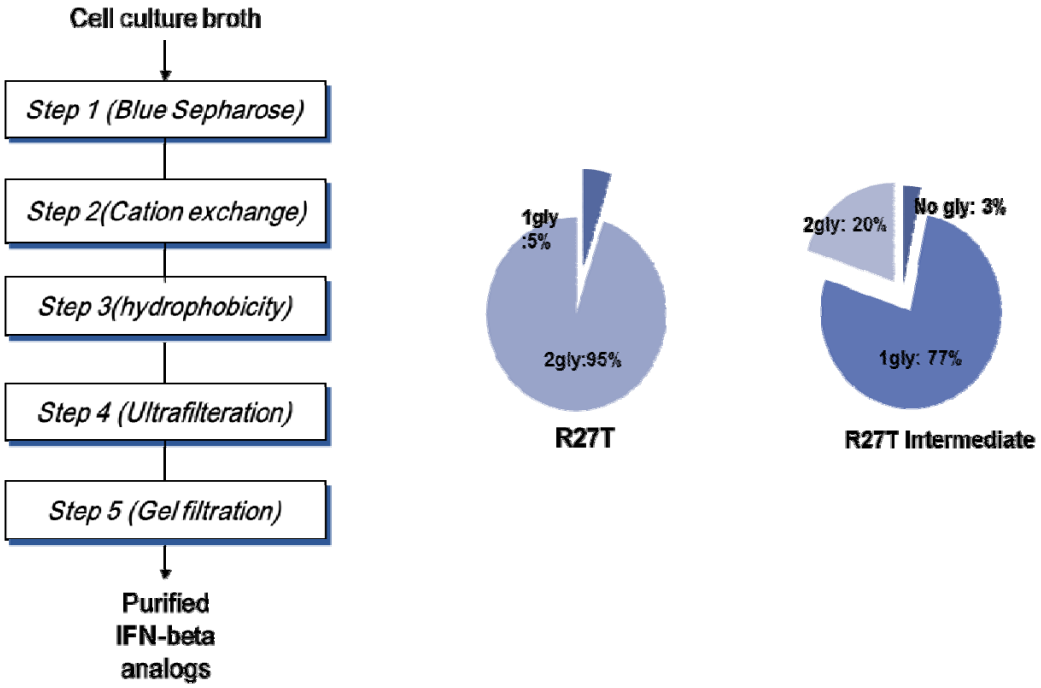

Figure 11. Initial purification process and purity of R27T.

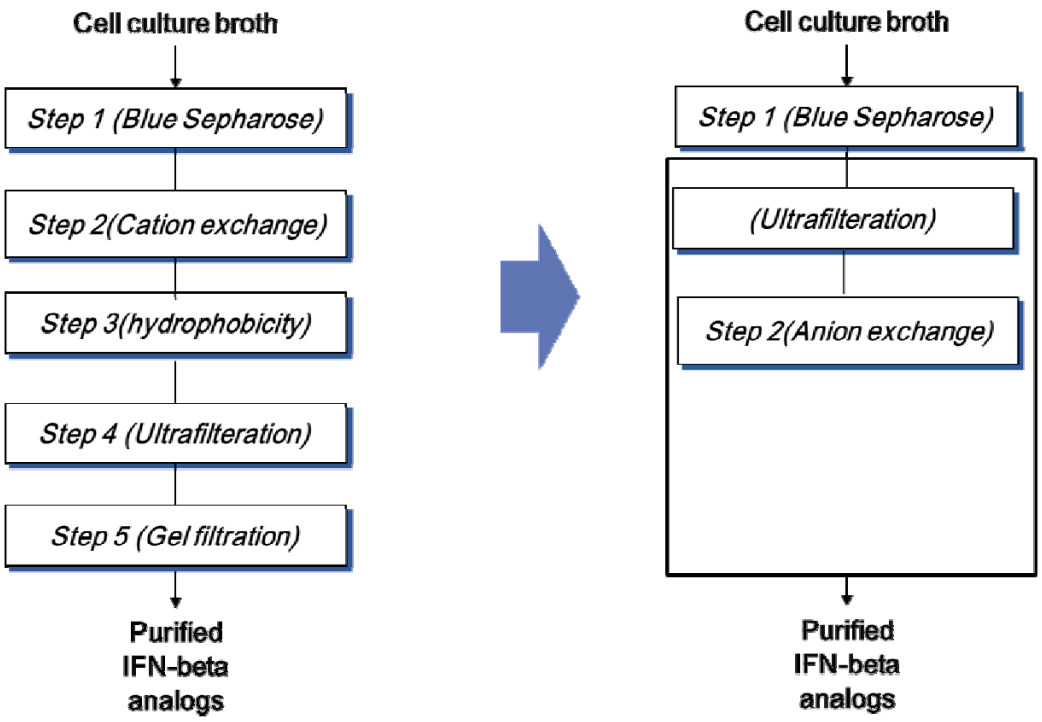

Figure 12. Improvement of the purification process.

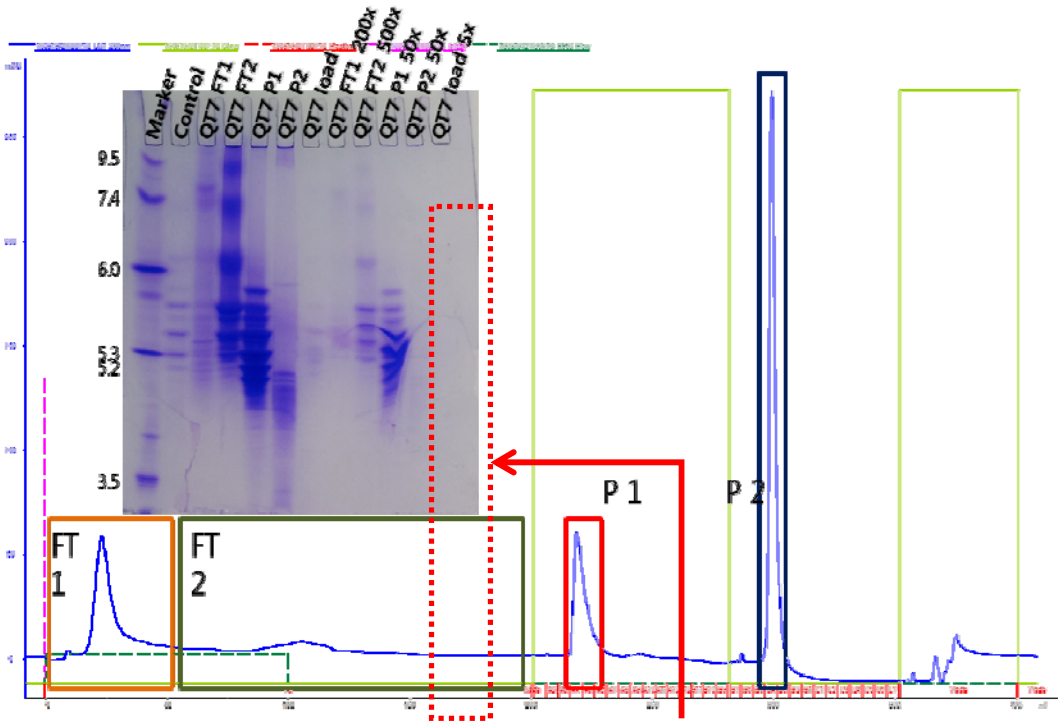

Figure 13. Product qualification with IEF.

4. Glycosylation site confirmation of R27T analogs with additional glycosylation

The specific sites of glycosylation were conclusively confirmed by the determination of the respective carbohydrate attachment sites to the polypeptide backbone of proteins. Analyses were performed on a trypsin/Glu-C digest of R27T and the control protein Rebif to identify glycopeptides using quadrupole-TOF (Q-TOF) mass spectrometry, in which C3 and C13 peptide fragments have possible glycosylation site at Asn25 and Asn80 for R27T and Asn80 for Rebif (Figure 14A, 14B). The glycopeptide ions were extracted and confirmed by the presence of oxonium ion, such as *m/z* 204 (HexNAc) and 366 (HexHexNAc) at 21 min and 46 min in the extracted ion chromatogram (Figure 15A). The presence of oxonium ion was analyzed again in the product ion spectrum at 21 min and 46 min (Figure 15B). The identification of N-glycosylation sites by mass spectrometry was often permitted from the specific deamidation of asparagines to aspartic acid within the consensus sequence NX (S/T) upon cleavage of the glycan moiety by PNGase F. Deglycosylated peptide was sequenced by LC/MS/MS (Figure 15C).

A

1 10 20 30
M S Y N L L G F L Q R S S N F Q C Q K L L W Q L N G R L E Y

31 40 50 60
C L K D R M N F D I P E E I K Q L Q Q F Q K E D A A L T I Y

61 70 80 90
E M L Q N I F A I F R Q D S S S T G W N E T I V E N L L A N
C13 Glycopeptide

91 100 110 120
V Y H Q I N H L K T V L E E K L E K E D F T R G K L M S S L

121 130 140 150
H L K R Y Y G R I L H Y L K A K E Y S H C A W T I V R V E I

151 160 166
L R N F Y F I N R L T G Y L R N

B

1 10 20 30
M S Y N L L G F L Q R S S N F Q C Q K L L W Q L N G T L E Y
C3 Glycopeptide

31 40 50 60
C L K D R M N F D I P E E I K Q L Q Q F Q K E D A A L T I Y

61 70 80 90
E M L Q N I F A I F R Q D S S S T G W N E T I V E N L L A N
C13 Glycopeptide

91 100 110 120
V Y H Q I N H L K T V L E E K L E K E D F T R G K L M S S L

121 130 140 150
H L K R Y Y G R I L H Y L K A K E Y S H C A W T I V R V E I

151 160 166
L R N F Y F I N R L T G Y L R N

Figure 14. Amino acid sequence of Rebif (A) and R27T (B). Shadowed boxes on amino acid sequence indicate predicted glycopeptides and circles indicate potential glycosylation sites.

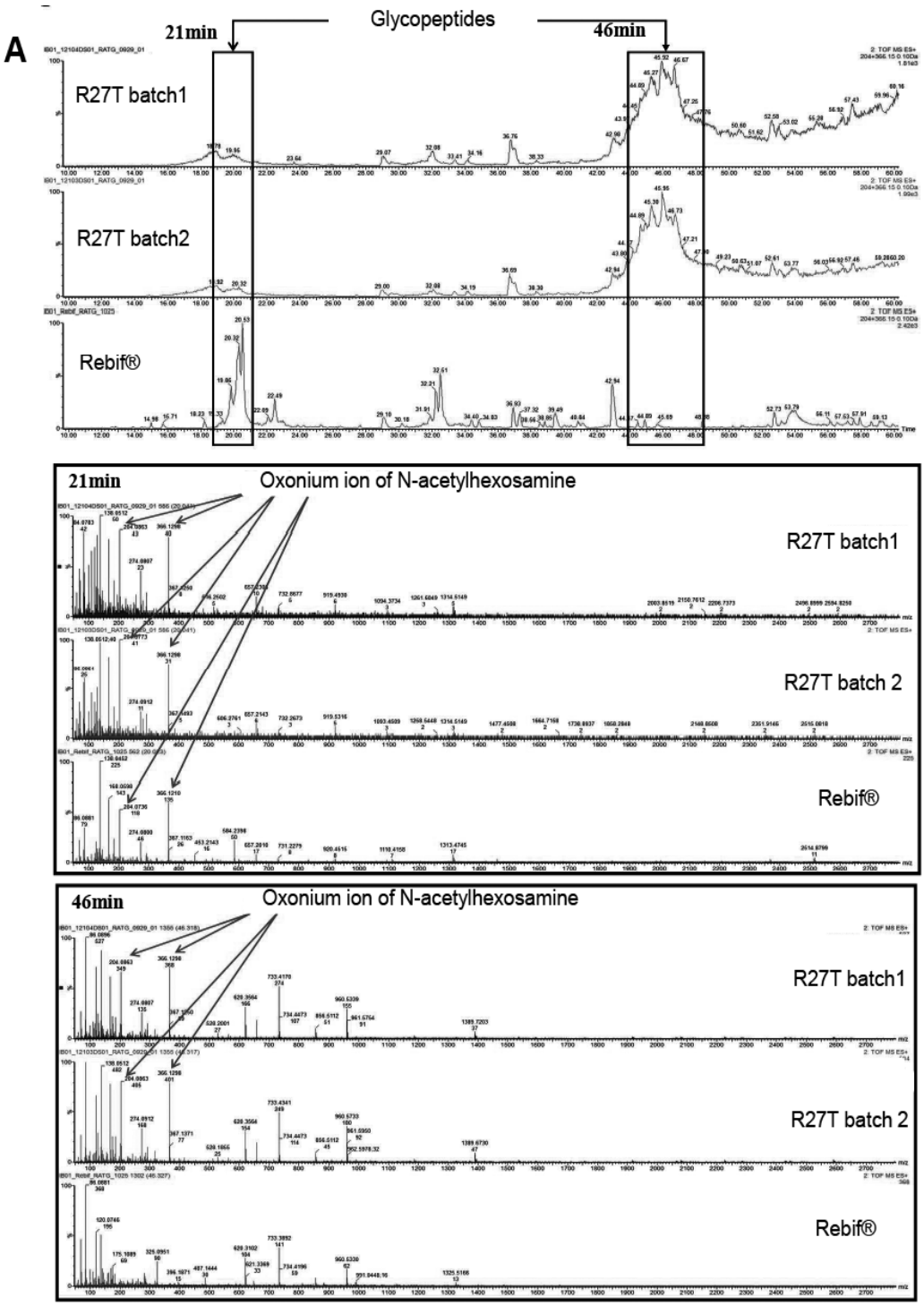
A
Glycopeptides
21min
46min
R27T batch1
R27T batch2
Rebif®
21min
Oxonium ion of N-acetylhexosamine
R27T batch1
R27T batch 2
Rebif®
46min
Oxonium ion of N-acetylhexosamine
R27T batch1
R27T batch 2
Rebif®

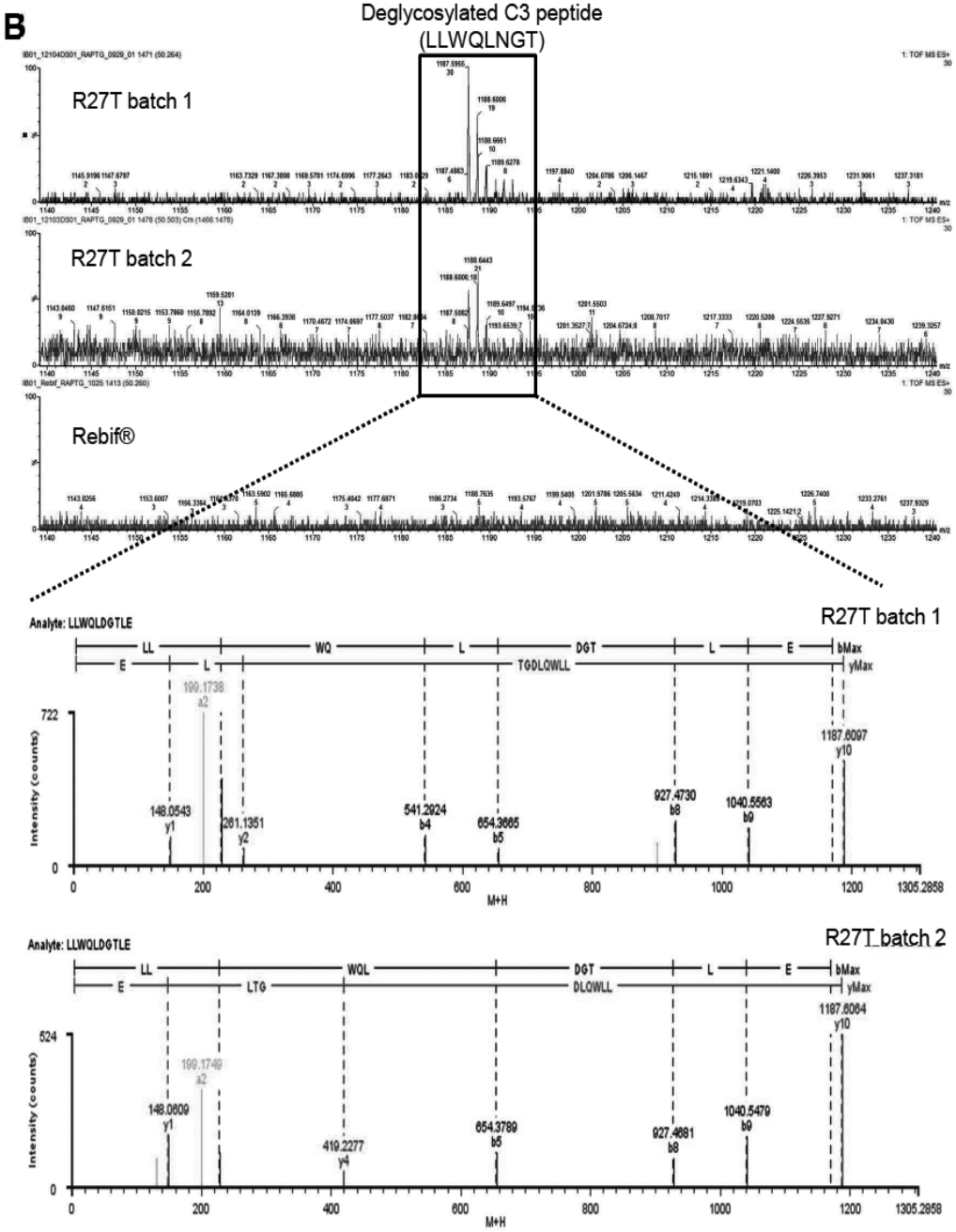
B
Deglycosylated C3 peptide
(LLWQLNGT)
R27T batch 1
R27T batch 2
Rebif®
Analyte: LLWQLDGTLE
R27T batch 1
LL
WQ
L
DGT
L
E
bMax
E
L
TGDLQWLL
yMax
199.1738
a2
722
Intensity (counts)
1187.6097
y10
148.0543
y1
261.1351
y2
541.2924
b4
654.3685
b5
927.4730
b8
1040.5563
b9
0
200
400
600
800
1000
1200
1305.2858
M+H
Analyte: LLWQLDGTLE
R27T batch 2
LL
WQL
DGT
L
E
bMax
E
LTG
DLQWLL
yMax
1187.6064
y10
524
Intensity (counts)
199.1749
a2
148.0609
y1
419.2277
y4
654.3789
b5
927.4681
b8
1040.5479
b9
0
200
400
600
800
1000
1200
1305.2858
M+H

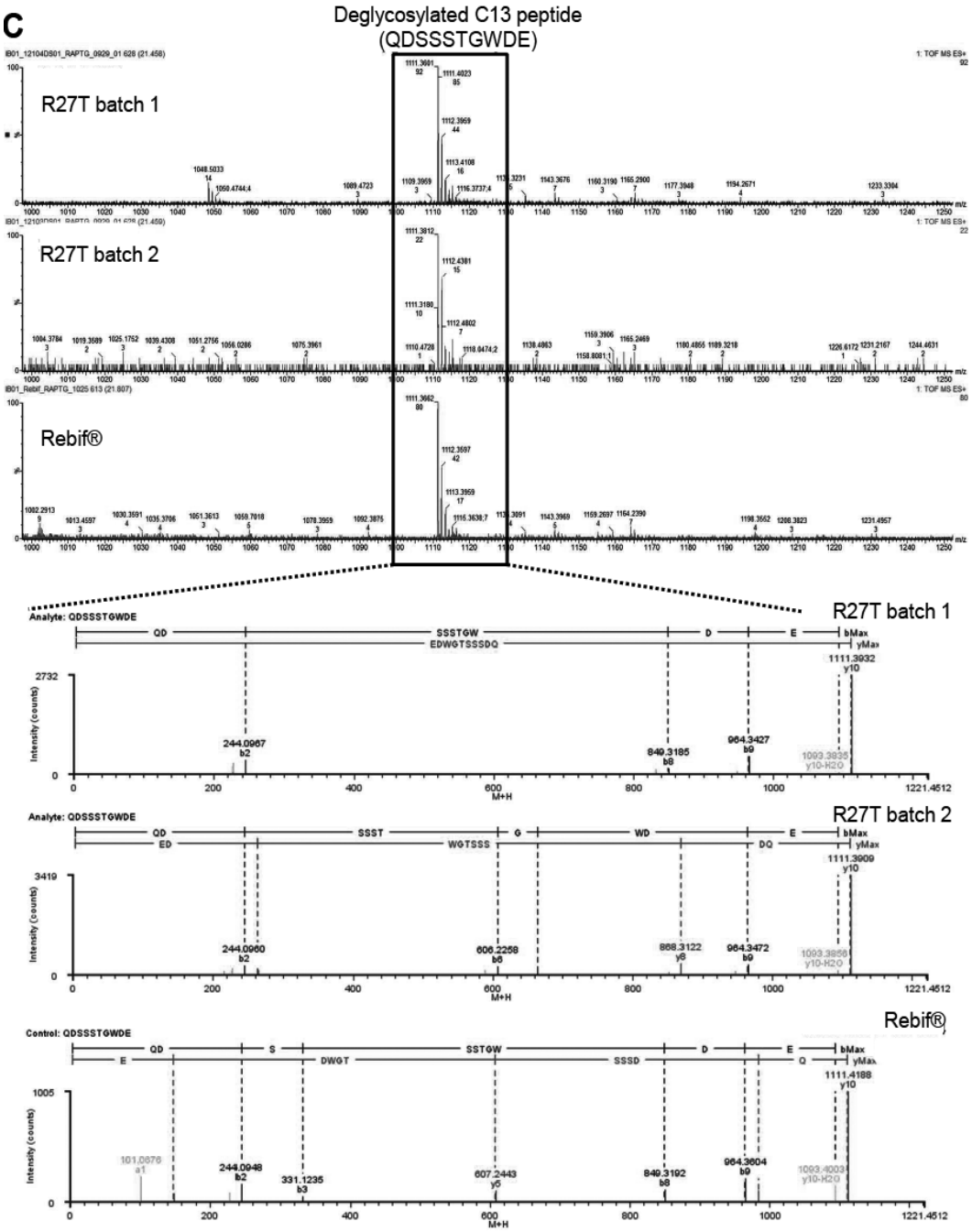
C
Deglycosylated C13 peptide
(QDSSSTGWDE)
R27T batch 1
R27T batch 2
Rebif®
Analyte: QDSSSTGWDE
R27T batch 1
Analyte: QDSSSTGWDE
R27T batch 2
Control: QDSSSTGWDE
Rebif®
Intensity (counts)
M+H

Figure 15. LC/ESI MS/MS of trypsin/Glu-C digests of R27T and Rebif. (A) Extraction ion chromatogram at m/z 204 and 366 for product ion spectra at 21 min and 46 min, respectively. Amino acid sequencing of deglycosylated C3 and C13 peptides by LC/ESI MS/MS. (B) Deglycosylated C3 peptide MS spectrum and fragmentation information for R27T (Lot:12104DS01 and 12103DS01) and Rebif. (C) MS spectrum of the deglycosylated C13 peptide and fragmentation information for R27T (Lot:12104DS01 and 12103DS01) and Rebif.

5. The analysis of glycosylation

Glycans have a very prominent role in influencing the therapeutic efficacy and determination of the *in vivo* half-life of therapeutic proteins. Glycosylation analysis of the relative proportions of monosaccharide contents of R27T compared to the reference protein Rebif was performed. Individual sugar residues were identified and quantitated on a mole per mole basis in which the monosaccharide contents in 1 mol of R27T and Rebif were determined using a standard curve (Table 5). All carbohydrate moieties consisted of fucose, *N*-acetylglucosamine, galactose, mannose, and sialic acid without *N*-acetylgalactosamine. Therefore, they showed N-linked complex-type sugar chains.

Table 5. Sugar composition analysis of R27T and Rebif

(mol/mol protein)

	Fucose[a]	N-acetyl-glucosamine[b]	N-acetyl-galactosamine[b]	Galactose[a]	Mannose[a]	Sialic acid[c]
R27T	2.4	12.3	N.D.	7.7	7.1	3.2
Rebif	1.1	4.7	N.D.	3.0	3.5	1.2

[a] 2M TFA for neutral sugars at 100ºC at 4 h

[b] 6N HCl for amino sugars at 100ºC at 4 h

[c] 0.1N HCl for sialic acids(NANA+NGNA) at 80ºC at 1 h

The MALDI spectra from the permethylated N-glycans indicated that the majority of the glycans were core fucosylated bi-antennary glycans (FA2G2; H5N4F1) with 0, 1, or 2 sialic acids. Masses corresponding to core fucosylated tri-antennary glycans (FA3G3; H6N5F1) with 1, 2, or 3 sialic acids were also detected. The spectra from the positive and negative controls are shown in Figure 16.

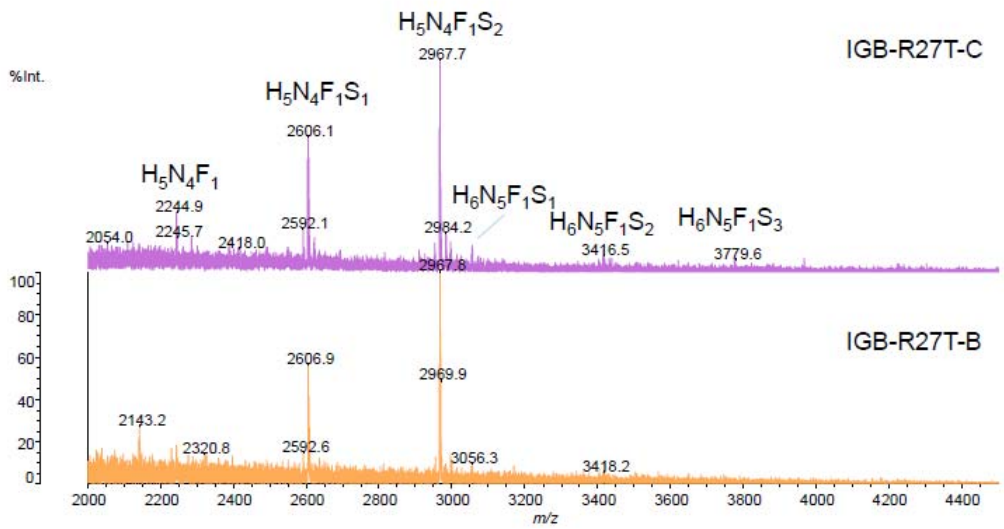

Figure 16. MALDI spectra from permethylated R27T samples

m/z [M + Na] +.H = hexose, N = *N*-acetylhexosamine, F = fucose (deoxyhexose). No peaks were detected in release-A (data not shown).

The sample was further analyzed to confirm the proposed structures. Anion exchange chromatography of 2-AB-labeled glycans was performed to separate glycans based on charge, including mono-, di-, tri-, and tetra sialylated glycans, and revealed the relative amounts of sialic acid on the glycan (Figure 17). The molar ratios of each N-glycan calculated from the peak areas were 26.14%, 35.60%, 21.66%, and 16.59% in mono-, di-, tri-, and tetra-sialyated glycan structures in R27T, respectively. The coefficient of variation (CV) on peak areas (as % of total area) for the analysis triplicate release was <2% on all peaks.

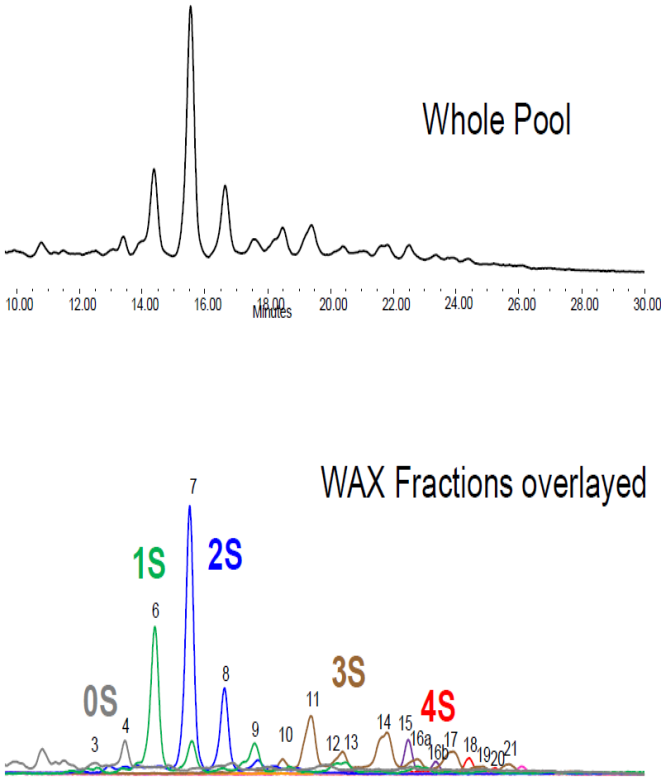

Figure 17. LugerSep-N2 HILIC-HPLC profiles of R27T WAX fractions. Number of sialic acids: 0S in gray, 1S in green, 2S in blue, 3S in brown, and 4S in red.

Glycans were separated by WAX-HPLC into fractions containing 0, 1, 2, 3, or 4 sialic acids and then identified by HILIC-HPLC before and after sialidase digestion by correlation to GU values for structures identified in the sample by exoglycosidase sequencing. Comparison of the sialidase-only digestion with the sialidase plus fucosidase digestion revealed that the majority of peaks moved by approximately 0.4 GU units in line with the loss a core α-1-6 fucose. The relative amount of core fucosylated structures was 94%. Comparison of the sialidase plus fucosidase digestion with the sialidase plus fucosidases plus β-galactosidase digestion revealed that a number of peaks digested to the core antennary structures A2, A3, A3′, and A4. However, a number of peaks did not digest down to these core structures until *N*-acetylglycosaminidase (sph) was also added. This was because they contained a lactosamine extension. The lactosamine extension can be added onto any antenna, and so there were a number of different isomeric structures possible. The data from the sialidase plus fucosidases and galactosidase exoglycosidase digestion could be used to assign the different amounts of antennary structures that were present within the sample. This combination of enzymes digested the structures down to the core A2, A3, A3′, and A4 structure for which the GU values were well documented. Structures that did not digest down to these cores contained a lactosamine extension (Table 6).

Table 6. LugerSep-N2 peaks with GU values and structures determined from WAX fractions. The additional possible lactosamine structures are listed in italics

Peak id	R27T-A,B,C G-L1-N Average GU	R27T-A,B,C G-L1-N Average % Area	R27T G-L2-N Whole Pool GU	R27T G-L2-N Whole Pool % Area	R27T WAX Fractions: Major Structure GU	Major Structure	Other Structures GU		GU		GU	
1	6.94	0.42	-	-								
2	7.11	0.36	7.18	0.74	7.2	A2G2						
3	7.26	0.07	7.42	0.80								
4	7.57	2.49	7.56	2.45	7.6	FA2G2						
5	7.80	1.96	7.97	15.99	8.0	FA2G2S1						
6	8.02	9.82										
7	8.54	25.36	8.46	39.85	8.4	FA2G2S2						
8	9.01	9.27	8.92	12.42	8.9	FA2G2S*2						
9	9.39	4.02	9.31	3.71	9.3	FA3'G3S1						
10	9.81	7.22	9.70	6.75	9.7	FA3G3S3						
11	10.25	8.31	10.10	6.48	10.1	FA3'G3S3						
12	10.69	3.85	10.55	1.56	10.6	FA3'G3S*3						
13	10.96	3.86	10.85	0.82	10.6	FA4G4S1						
14	11.36	6.43	11.20	2.82	11.2	FA4G4S3						
15	11.73	5.45	11.53	2.36	11.5	FA4G4S4						
16a	12.14	2.70	11.94	1.13	11.7	FA4G4S*3						
16b			12.13		11.9	FA4G4S*4						
17	12.38	2.74	12.21	0.64	12.2	FA4G4Lac1S3						
18	12.68	2.81	12.45	0.86	12.4	FA4G4S*4						
19	13.11	1.10	12.87	0.10	12.7	FA4G4Lac1S*3						
20	13.31	0.71			12.9	FA4G4Lac1S4						
21	13.59	0.76	13.35	0.19	13.2	FA4G4Lac2S3						
22	>13.7	0.32	>13.4	-	13.6	FA4G4Lac2S*3	*13.6*	*FA3G3Lac3S*3*	13.7	FA4G4Lac2S*4	14.2	FA4G4Lac3S4

	neutral
	1 sialic acid
	2 sialic acids
	3 sialic acids
	4 sialic acids
*	contains α2-6 linked sialic acid(s)

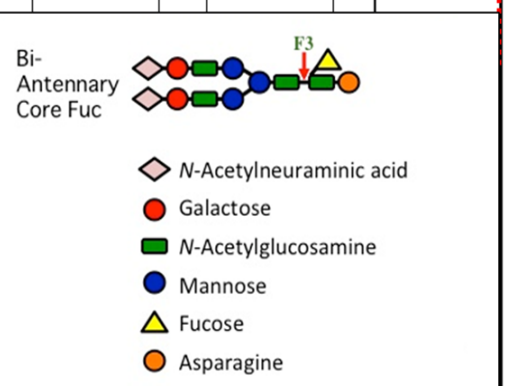

The structures were identified from the GU values in relation to the neutral structures that had been identified by exoglycosidase sequencing. Both forms of tri-antennary glycans were identified: A3G3 where the third GlcNAc was β1-4 linked to the 3-linked mannose and A3′G3 where the third GlcNAc was β1-6 linked to the 6-linked mannose. The lactosamine extension on a structure added approximately the same value to the GU value as the addition of an extra antenna (both are Gal-GlcNAc). This means, for example, that a bi-antennary with two lactosamine extensions would have a similar GU value to a tri-antennary glycan with one lactosamine or a tetra-antennary with no lactosamine extensions. On the assumption that only one sialic acid was bound per terminal galactose, then the tetra-sialylated glycans were all tetra antennary (with or without lactosamine extensions). The tri-sialylated glycans could be either tri- or tetra-antennary glycans, whilst the di-or mono-sialylated glycans could be bi-, tri-, or tetra-antennary structures (with or without lactosamine extensions).

6. Protein stability measurement by biophysical analysis

DSC thermograms of rhIFN-β 1a and R27T in 20 mM acetate buffer, pH 4.2, were evaluated to determine thermal unfolding events (Figure 18). Unfolding transition temperature (T_m), calorimetric enthalpy (ΔH), and van't Hoff enthalpy (ΔH_v) of rhIFN-β 1a were 61.90°C, 39.88 kcal/mol, and 106.3 kcal/mol, respectively. In addition, T_m, ΔH, and ΔH_v of R27T were 59.07°C, 36.87 kcal/mol, and 103.6 kcal/mol, respectively. R27T exhibited lower T_m than rhIFN-β 1a, but had almost the same ΔH and ΔH_v. Although the T_m of R27T was approximately 2°C less than that of rhIFN-β 1a, R27T did not exhibit any visible aggregation after withdrawal from the DSC scan (no data).

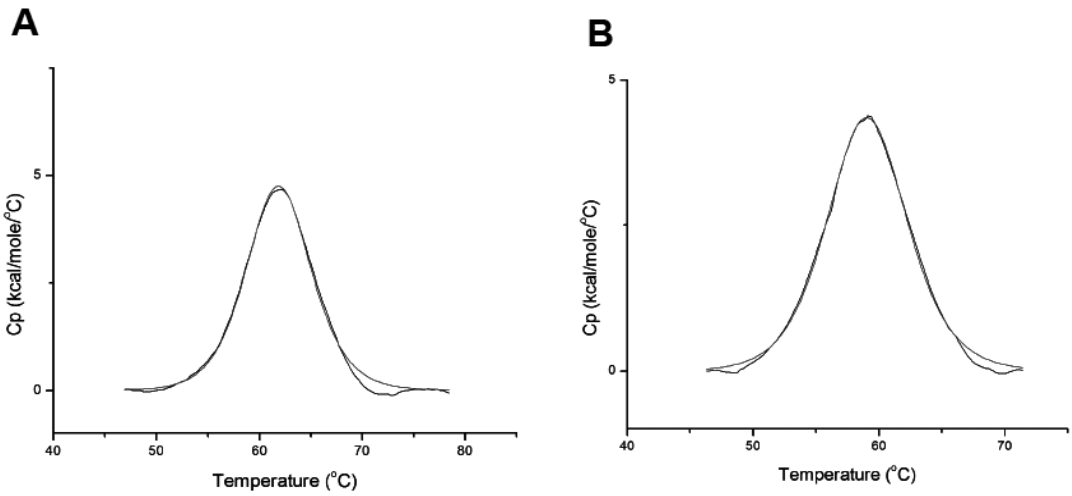

Figure 18. DSC thermograms of (A) rhIFN-β 1a and (B) R27T. Measured T_m values are displayed above the peaks. Graphs also show curve fitting of the DSC thermograms for rhIFN-β 1a and R27T, which was performed using a non-two-state model.

DLS was used to observe hydrodynamic size of rhIFN-β 1a and R27T and the existence of aggregates in the aqueous environment (Figure 19). rhIFN-β 1a produced two significant volume distribution peaks at 2.700 nm and 9.825 nm with 98.9% and 1.3% volume ratio, respectively. However, R27T had only a single-size distribution peak at 3.722 nm. This indicated the existence of aggregation issues with rhIFN-β 1a. The polydispersity index (PDI) values of rhIFN-β 1a and R27T were 0.607 and 0.306, respectively. Since rhIFN-β 1a has a higher PDI value, the protein was more polydispersed and might not be stable in the aqueous environment as compared to R27T. Therefore, the result may indicate that rhIFN-β 1a is less stable in the aqueous solution than R27T.

In order to investigate the secondary structural stability of the proteins, ATR FT-IR was selected to analyze the amide group I (1,700 cm^{-1}~1,600 cm^{-1}) in proteins. The amide group I region of the ATR-FTIR spectra was separated into nine peaks with Fourier self-deconvoluted spectra of rhIFN-β 1a and R27T. Each ratio of the composite area represents the corresponding percentage of each structure from peak 1 to 9: peak #1, 2, 6, and 7 (1,692 cm^{-1}, 1,676 cm^{-1}, 1,636 cm^{-1}, and 1,623 cm^{-1}, respectively; β-sheet), peak #3 (1,665 cm^{-1}; reverse turn), peak #4 (1,655 cm^{-1}; α-helix), peak #5 (1,646 cm^{-1}; random coil), peak #8 (1,615 cm^{-1}; side chain vibration), and peak #9 (1,598cm^{-1}; β-turn) were resolved accordingly. After resolving the peaks, the relative percentage of the contents was calculated. Table 7 shows the relative ratio of α-helix, β-sheet, β-turn, and random coil of rhIFN-β 1a and R27T. R27T contains more α-helix and less β-sheet than rhIFN-β 1a. Recent spectroscopy

studies suggested that increased intermolecular β-sheet structure was a common feature of protein aggregation, although IFN consists of only α-helix [32-34]. The β-sheet content of rhIFN-β 1a was about 5% higher than R27T, which suggested nonnative protein aggregation [33].

To confirm the actual effect of stability, the aggregation kinetics were observed (Figure 19C). The CPE assay was used to detect bioactivity of R27T and rhIFN-β 1a in accelerated condition 37°C for up to 96 h. The bioactivity with aggregation of R27T compared with rhIFN-β 1a decreased within the first 96 h. The calculated half-life for rhIFN-β 1a was 96 h, in contrast to 503 h for R27T.

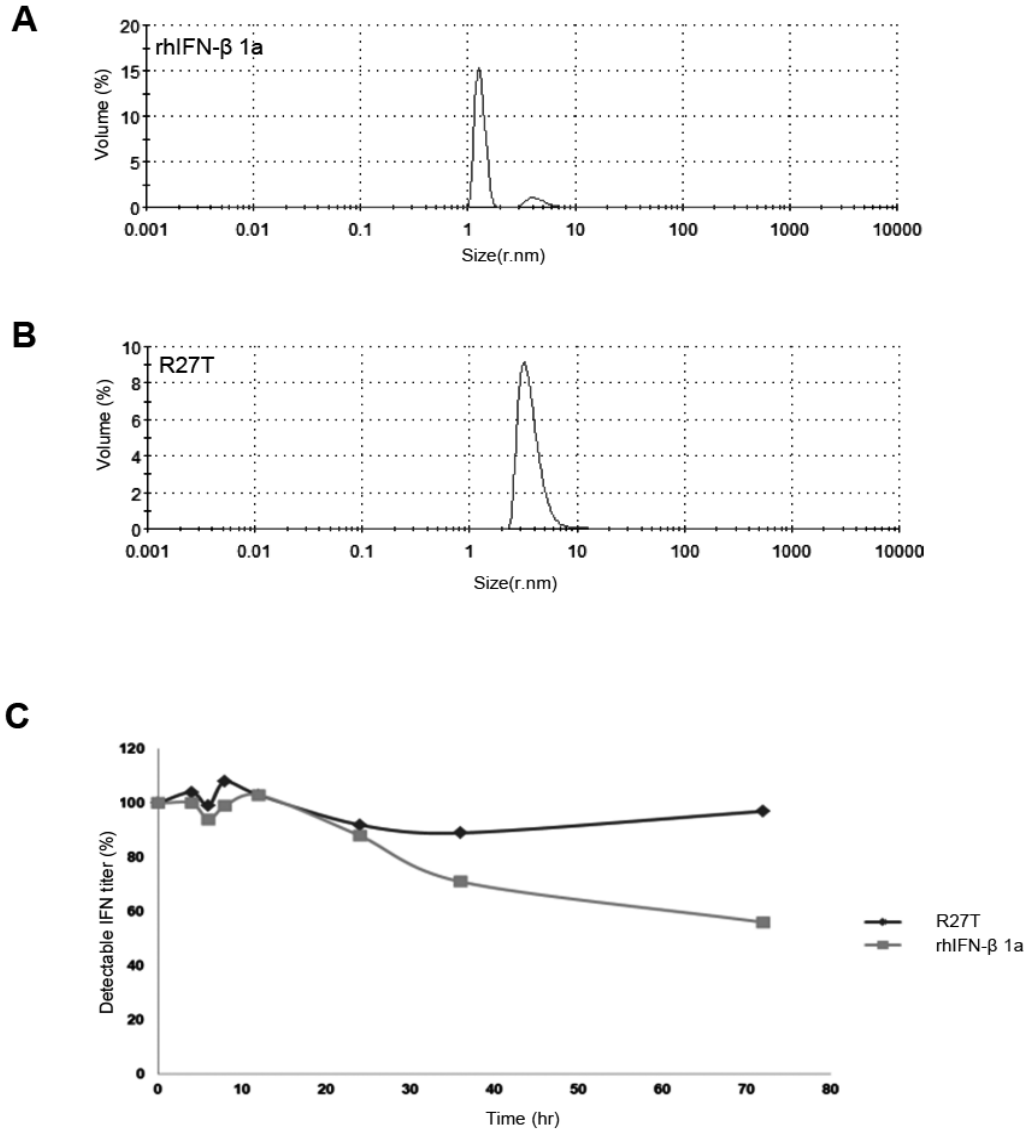

Figure 19. Size distribution of (A) rhIFN-β 1a and (B) R27T. The analysis was performed at a scattering angle of 90°. Distributed sizes, PDI, and Zeta averages are shown. (r.nm, radius in nanometers). (C) IFNs were quantified by CPE at various intervals up to 72 h.

Table 7. Secondary structure ratios derived from the ATR-FTIR spectra of rhIFN-β 1a and R27T in solution

Samples	Amide I region in ATR FTIR spectra			
	α-helix (%)	β-sheet (%)	β-Turn (%)	Random Coil (%)
rhIFN-β 1a	17.3	37.0	24.5	21.2
R27T	29.8	31.3	25.6	13.3

7. Maintenance of *in vitro* activity

From the purification process, mixed R27T, which is the mixture of mono- and di-glycosylated R27T in the ratio of 3:7, was purified and analyzed with R27T and Rebif for this assay (data not shown). 299×10^6, 252×10^6, and 288×10^6 IU/mg were obtained from average activity of three lots of R27T, two lots of mixed R27T, and Rebif, respectively (Figure 20A). There was no loss of anti-viral activity with additional glycosylation. The relative potencies of R27T, mixed R27T, and Rebif in anti-proliferative and immune modulation assays were also examined. Similar activity differences were observed in these assays as well. In the anti-proliferative assay, IC50s of 14, 22, and 29 pg/mL were obtained from R27T, mixed R27T, and Rebif, respectively (Figure 20B). In a FACS assay, measuring IFN-inducible expression of MHC class I on the surface of A549 cells, 50% responses were observed at approximately 265 (R27T), 359 (mixed R27T), and 238 pg/mL (Rebif) (Figure 20C).

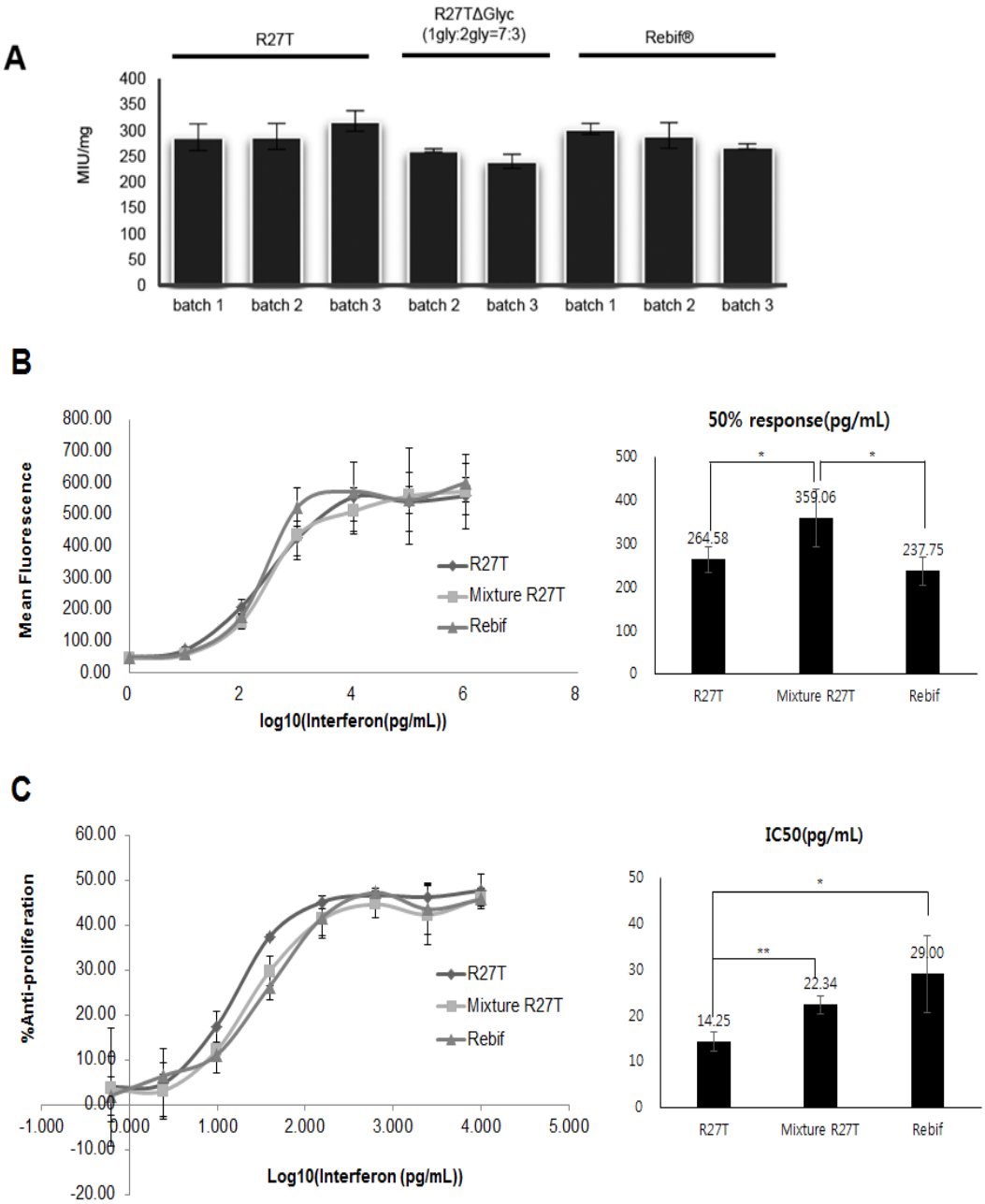

Figure 20. *In vitro* activity. (A) Anti-viral, (B) anti-proliferative, and (C) immunomodulatory activities of R27T (◆), R27TΔGlyc (■) and Rebif (▲).

8. Molecular modeling of the R27T/IFNAR2 complex

On the basis of the crystal structure of human IFN-β 1a, a structure for R27T was generated *in silico*, in which bulky glycosylation was used with one of the main structures obtained from HILIC profiles of R27T (FA2G2S2, F: Core fucosylated, A2: biantennary with both GlcNAcs as β1-2 linked, G2: two galactose-linked β1-4 to antenna, S2: two sialic acids linked to galactose). The known IFN-α2/IFNAR2 docking structure was used as a template structure because of the structure similarity of about 30% between IFN-α2 and IFN-β 1a. The R27T/IFNAR2 docking structure is shown in Figure 19A. N-glycosylation was predicted to attach at the 80th amino acid easily regardless of oligosaccharide structure or lengths (solvent-accessible surface area 76.7A by NACCESS) in which glycosylation could have no effect on the R27T/IFNAR2 complex due to the distance between the oligosaccharide and receptor [35]. On the other hand, glycosylation on the 25th amino acid was likely to be more difficult than the 80th glycosylation based on *in silico* simulations, as the 25th amino acid side chain was orientated toward the inside. However, it was confirmed that the structure of the glycosylation at the 25th residue could possibly be like that at the 80th residue through a "wet" experiment like SDS-PAGE (Figure 21B, 21C). From these results, the R27T structure with glycosylation at the 25th residue could be obtained and indicated that glycosylation of R27T could stabilize the interaction between R27T and IFNAR2. In particular, new hydrogen bond interactions were found between

44T and 51D of IFNAR2 and the oligosaccharide of R27T, resulting in increases in the stability of the R27T/IFNAR2 complex (Figure 8B). Similarly, hydrogen bonding between 35R of R27T and oligosaccharide could contribute to the overall stability of the helical conformations of R27T (Figure 21C).

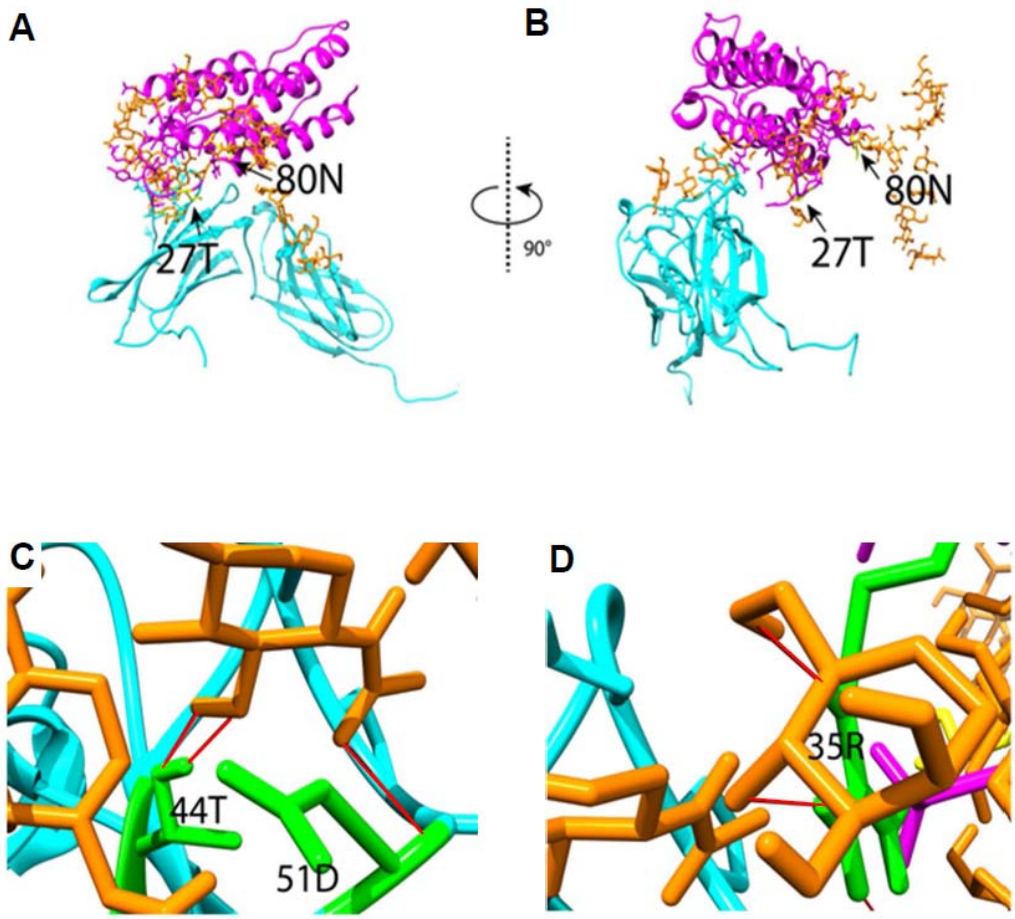

Figure 21. Model of the N-glycosylated R27T/IFNAR2 complex. (A) Front view and (B) side view. The complex structure oligosaccharides, R27T, and IFNAR2 are shown as orange, magenta, and cyan, respectively. New hydrogen bonds between the oligosaccharide and complex are presented as red bold lines in C (with IFNAR2), and D (R27T). Further, 27T and 80N in the R27T protein are colored by yellow (A, B) and hydrogen-bonded residues in R27T and IFNAR2 are colored green (C, D).

9. *In vivo* pharmacokinetic study in rats

The plasma concentration–time profiles of rhIFN-β after IV, SC, and IM administration of R27T, mixed R27T, and Rebif at a dose of 1 MIU/kg to rats are shown in Figure 22 and relevant pharmacokinetic parameters are listed in Table 8. After IV administration of the three rhIFN-βs formulations, bi-exponential declines in plasma rhIFN concentrations were observed. The AUC values of R27T were significantly higher than those of mixed R27T and Rebif by 1.47- and 1.36-fold, respectively. Thus, the CL values were significantly reduced in R27T compared to the other rhIFN-β formulations. Moreover, the $t_{1/2}$ values of R27T tended to be higher than those of the other rhIFN-β formulations by 1.39- and 1.44-fold, respectively. The V_{ss} values were comparable among the three rhIFN-β formulations. After SC administration, the AUC and F values of R27T were significantly higher than those of mixed R27T by 2.95- and 2.01-fold, respectively, and those of Rebif by 2.33- and 1.72-fold, respectively. Moreover, the $t_{1/2}$ values of R27T tended to be higher than those of mixed R27T and Rebif by 1.71- and 2.35-fold, respectively. The C_{max} and T_{max} values were comparable among the three rhIFN-β formulations. After IM administration, the AUC and F values of R27T were significantly higher than those of mixture R27T by 2.36- and 1.58-fold, respectively, and those of Rebif by 2.24- and 1.65-fold, respectively. The $t_{1/2}$ values of R27T and mixed R27T were significantly higher than those of Rebif by 2.84- and 3.56-fold, respectively. The C_{max} values of mixture R27T were significantly lower than those of R27T and Rebif,

and the T_{max} values were comparable among the three rhIFN-β formulations. The $t_{1/2}$ values after SC and IM administration were much higher than those after IV administration, indicating that the each substance is subject to flip-flop kinetics.

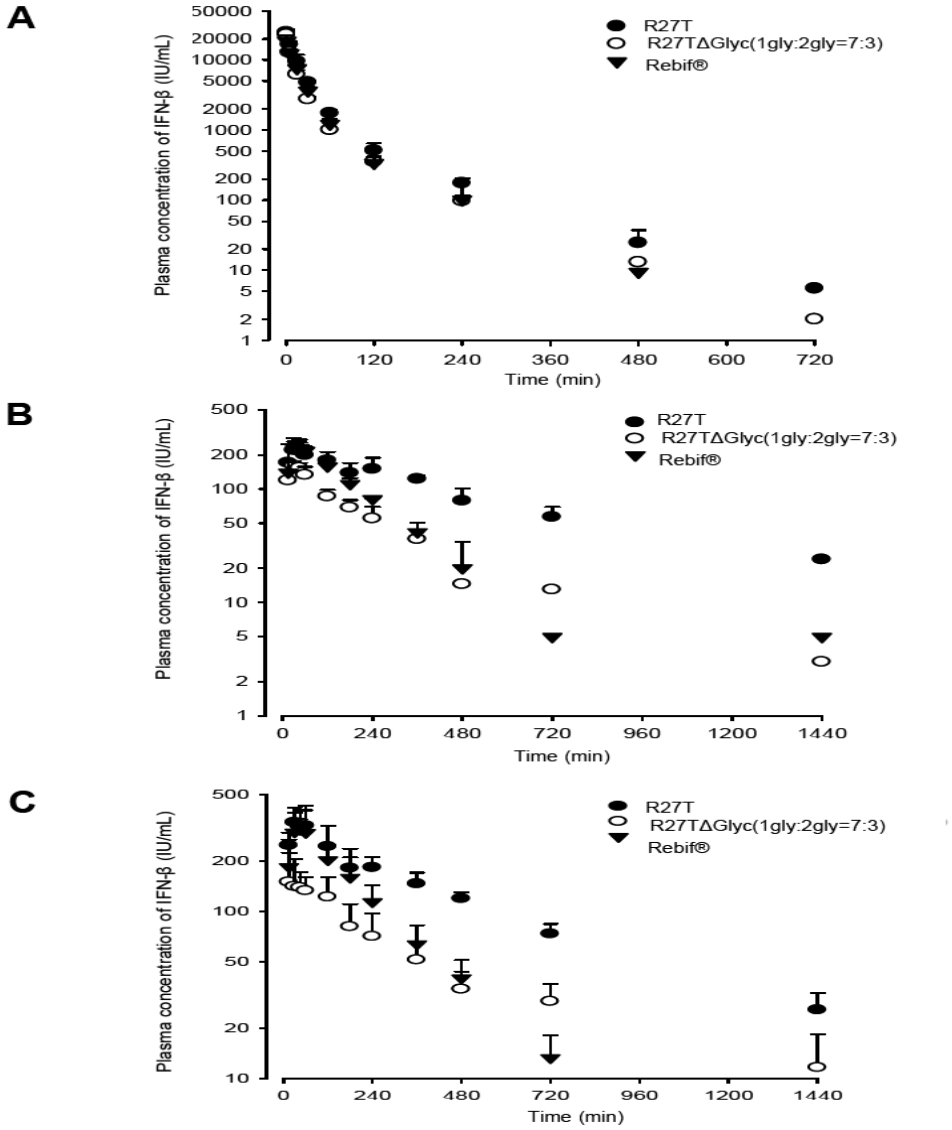

Figure 22. Mean arterial plasma concentration-time profiles for rhIFN-β after (A) intravenous, (B) subcutaneous, and (C) intramuscular administration of R27T, R27TΔGlyc, and Rebif at a dose of 1 MIU/kg in rats. Vertical bars indicate standard deviations (n = 3).

Table 8. Pharmacokinetic parameters after intravenous (IV), subcutaneous (SC), and intramuscular (IM) administration of R27T, R27TΔGlyc, and Rebif at a dose of 1 MIU/kg to rats (n = 3).

Parameters	R27T	R27TΔGlyc	Rebif
		IV	
AUC ($\times 10^4$ IU·min/mL)	54.8 ± 7.4*	37.2 ± 2.1	40.3 ± 2.4
$t_{1/2}$ (min)	88.0 ± 4.4	63.3 ± 11.5	61.3 ± 21.6
CL (mL/min/kg)	1.9 ± 0.2*	2.7 ± 0.1	2.5 ± 0.2
V_{ss} (mL/kg)	90.1 ± 8.7	110 ± 17.1	107 ± 36.2
		SC	
AUC ($\times 10^4$ IU·min/mL)	12.2 ± 1.5*	4.1 ± 1.3	5.2 ± 0.5
$t_{1/2}$ (min)	423 ± 154	247 ± 121	180 ± 69.3
C_{max} (IU/mL)	235 ± 54.0	161 ± 14.9	246 ± 42.0
T_{max} (min)	30 (15-45)	30 (30)	45 (30-45)
F (%)	22.3	11.1	13
		IM	
AUC ($\times 10^4$ IU·min/mL)	16.3 ± 2.0*	6.9 ± 1.3	7.3 ± 2.1
$t_{1/2}$ (min)	426 ± 44.7	534 ± 211	150 ± 11.8*
C_{max} (IU/mL)	374 ± 59.7	172 ± 35.1*	314 ± 98.4
T_{max} (min)	45 (30-60)	15 (15-120)	45 (30-60)
F (%)	29.7	18.8	18

* Significantly different to the other groups ($p < 0.05$).

10. *in vitro* activity of PEG-R27T

To determine the effect of PEGylation on the specific antiviral activity, R27T, PEG-R27T were assayed in the A549 cell/EMCV virus CPE bioassay. Incorporation of a 20K and 40K PEG moiety at various sites produces an approximately 7- to 27-fold loss of specific activity compared to R27T (Figure 23). The relative potencies of R27T and 20K PEG-R27T in anti-proliferative and immune modulation assays were also examined. Similar activity differences were observed. Using FACS analysis, measuring IFN-inducible expression of MHC class I on the surface of A549 cells, 50% responses were observed at approximately 265 and 6,850 pg/mL, respectively (Figure 24A). In the anti-proliferative assay, IC50s of 14.3 and 220 pg/mL were obtained from R27T and 20K PEG-R27T, respectively (Figure 24B).

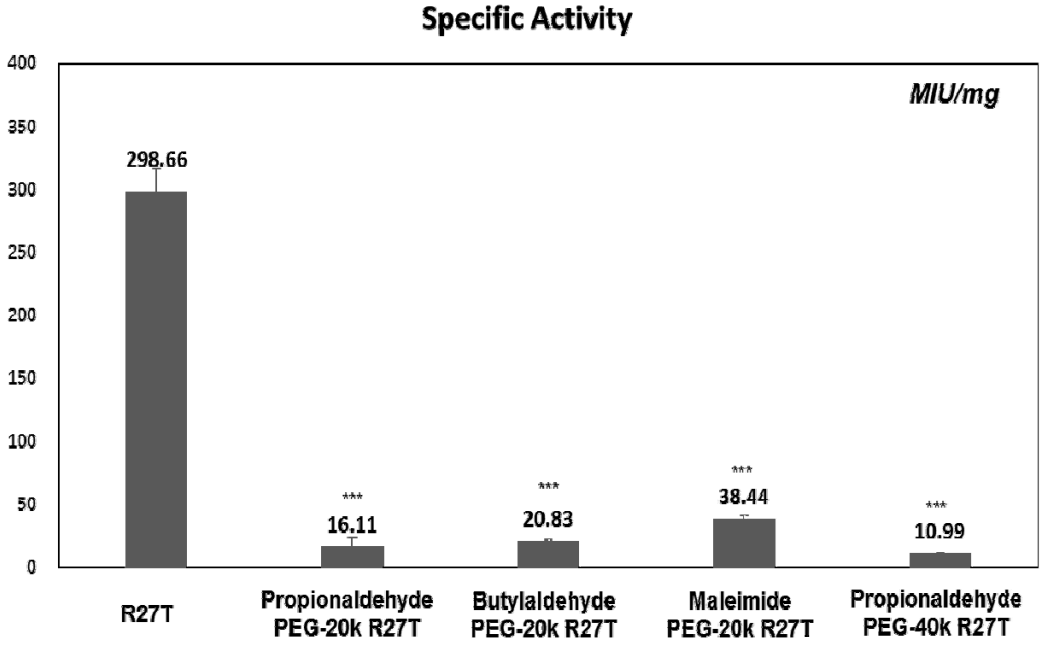

Figure 23. PEG-R27T antiviral activity.

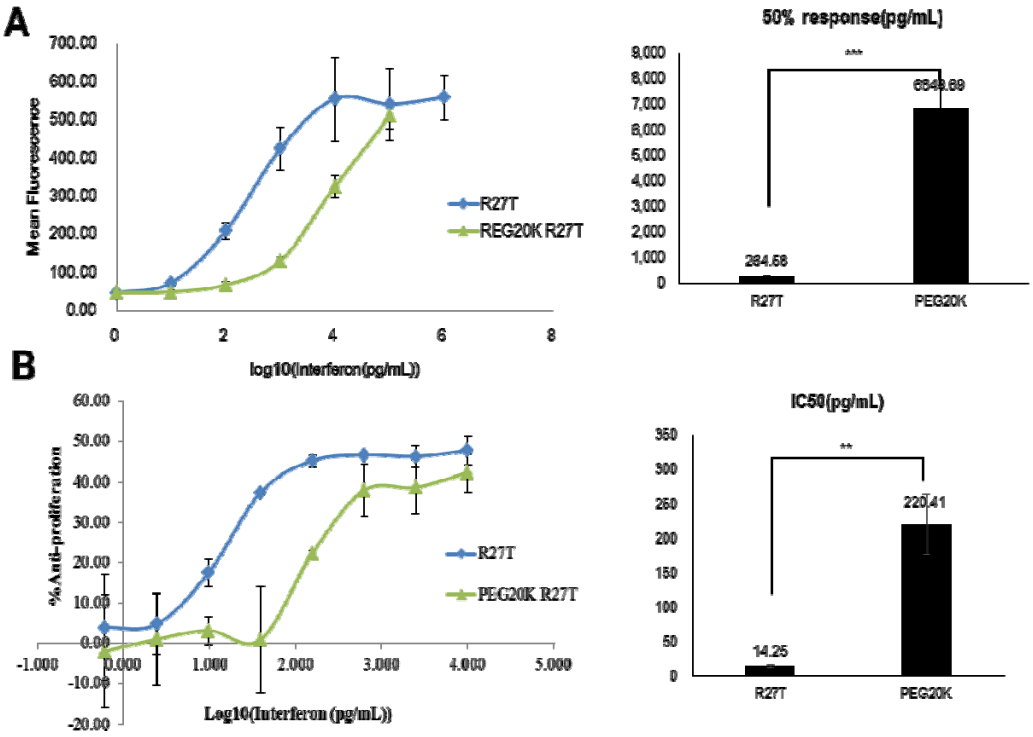

Figure 24. *In vitro* PEG-R27T activity.

11. *In vivo* PEG-R27T pharmacokinetic study in rats

The plasma concentration–time profiles of rhIFN-β 1a after IV, SC, and IM administration of R27T and two different PEGylated R27T formulations (PEG-R27Ts; PEG-20K and -40K) at a dose of 1 MIU/kg in rats are shown in Figure 25, and the relevant pharmacokinetic parameters are listed in Table 9. After IV administration of the three IFN formulations, mono- or bi-exponential declines in plasma IFN concentrations were observed. The AUC values of the PEG-R27Ts (PEG-20K and -40K) were significantly higher than those of R27T by 9.01- and 8.67-fold, respectively. Thus, the CL values were significantly reduced in the PEG-R27Ts compared with R27T. Moreover, the $t_{1/2}$ values of PEG-20K were significantly longer than those of R27T by 6.19-fold, and those of PEG-40K were further prolonged by 1.42-fold relative to PEG-20K. The V_{ss} values were in the following order: PEG-40K > PEG-20K > R27T. After SC administration, the AUC and F values of PEG-20K were significantly higher than those of R27T by 11.1- and 1.22-fold, respectively, and those of PEG-40K were further enhanced by 1.61- and 1.68-fold, respectively. Moreover, the $t_{1/2}$ values of PEG-40K were significantly higher than those of R27T and PEG-20K by 7.21- and 2.80-fold, respectively. The C_{max} and T_{max} values of the PEG-R27Ts were significantly higher than those of R27T. After IM administration, the AUC values of the PEG-R27Ts were significantly higher than those of R27T by 15.2- and 19.1-fold, respectively, and their F values by 1.69- and 2.21-fold, respectively. The $t_{1/2}$ values of PEG-20K and

PEG-40K tended to be longer than those of R27T by 3.78- and 4.62-fold, respectively. The C_{max} and T_{max} values of the PEG-R27Ts tended to be higher than those of R27T.

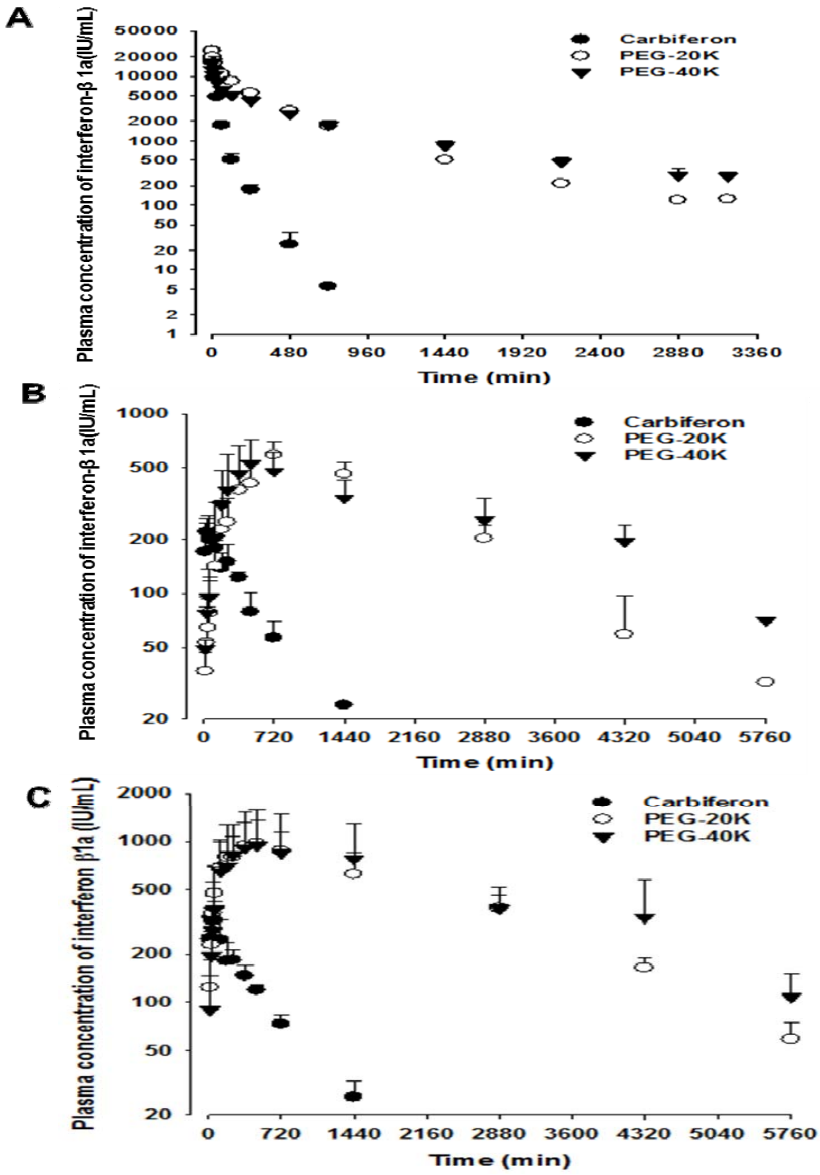

Fgure 25. Mean arterial plasma concentration–time profiles of rhIFN-β 1a after intravenous (A), subcutaneous (B), and intramuscular (C) administration of R27T, PEG-20K, and PEG-40K at a dose of 1 MIU/kg in rats. Vertical bars represent standard deviation (n = 3).

Table 9. Pharmacokinetic parameters of rhIFN-β 1a after intravenous (IV), subcutaneous (SC), and intramuscular (IM) administration of R27T, PEG-20K, and PEG-40K at a dose of 1 MIU/kg in rats (*n* = 3)

Parameters	R27T	PEG-20K	PEG-40K
	IV		
AUC ($\times 10^4$ IU·min/mL)	54.8 ± 7.42*	494 ± 18.7	475 ± 41.5
$t_{1/2}$ (min)	88.0 ± 4.35*	545 ± 27.0*	775 ± 91.3*
CL (mL/min/kg)	1.85 ± 0.242*	0.203 ± 0.00758	0.212 ± 0.0192
V_{ss} (mL/kg)	90.1 ± 8.69*	111 ± 2.21*	199 ± 11.7*
	SC		
AUC ($\times 10^4$ IU·min/mL)	12.2 ± 1.53*	135 ± 23.8*	218 ± 65.2*
$t_{1/2}$ (min)	423 ± 154	1090 ± 303	3050 ± 1370*
C_{max} (mL/min/kg)	235 ± 54.0*	595 ± 105	528 ± 187
T_{max} (mL/kg)	30 (15-45)	720 (360-720)	480
F (%)	22.3	27.3	45.9
	IM		
AUC ($\times 10^4$ IU·min/mL)	16.3 ± 2.01*	248 ± 66.0	311 ± 75.1
$t_{1/2}$ (min)	426 ± 44.7	1610 ± 797	1970 ± 1110
C_{max} (mL/min/kg)	374 ± 59.7	1050 ± 557	1020 ± 433
T_{max} (mL/kg)	45 (30-60)	720 (480-2880)	360 (240-1440)
F (%)	29.7	50.2	65.5

* Significantly different from the other groups ($p < 0.05$).

V. DISCUSSION

On the basis of patent information, as well as the knowledge of the structure-function studies of rhIFN-β 1a and type I IFN-β receptor protein, R27T, in which Thr (T) was substituted for Arg (R) at position 27 of rhIFN-β 1a, was constructed as a biobetter version of rhIFN-β 1a, resulting in the addition of a glycosylation site at residue 25. It was confirmed that glycoengineering successfully resulted in a protein with improved performance in bioassays, MS spectrometry, and *in vitro* activity. In particular, *in vitro* assays, including anti-viral, anti-proliferation, and immunomodulation, demonstrated that the additional glycosylation site at residue 25–27 exhibited no effect on ligand-receptor binding. However, these results conflicted with the results of Laura Runkel *et. al.* [36,37]. They suggested that residue 27, arginine, is one of the solvent-exposed residues (R) important for antiviral and reporter gene activity by alanine-scanning mutagenesis. Although alanine-scanning mutagenesis is a widely used technique in the determination of the functional role of proteins, mutagenesis of R27, having a polar R group, into alanine, a nonpolar, aliphatic R group, could result in a different effect than mutation to threonine, which also possesses a polar R group and results in the generation of a glycosylation site. In addition, glycosylation at residue 25 could affect the protein conformation without exerting an effect on receptor binding.

Glycosylation could also affect molecular stability. Stability issues, including aggregation, have been one of the biggest challenges for the development of therapeutic proteins at very different stages through production, purification, storage, and delivery. To address these issues, solution behavior of rhIFN-β 1a and

R27T was investigated with various biophysical methods, including DSC, DLS, and ATR FT-IR. Using DSC, thermal properties of the proteins were evaluated and the T_m difference of the proteins was found to be approximately 2°C. The conformational stability of R27T may be slightly lower than rhIFN-β 1a. Nevertheless, rhIFN-β 1a and R27T did not show a significant difference in thermal properties since $\Delta H_v/\Delta H$ values of rhIFN-β 1a and R27T were 0.38 and 0.36, respectively. They showed similar unfolding behavior when exposed to heat. However, studies of DLS and ATR FT-IR suggested that rhIFN-β 1a was more vulnerable to stability issues compared to R27T. Specifically, ATR FT-IR indicated that significant amounts of α-helical structures were highly retained while the amount of intermolecular β-sheet (indicative of aggregation) decreased upon the addition of a glycosylation site at residue 25. This result was consistent with DLS since aggregates were not observed. These results were also confirmed by the aggregation kinetic profile, demonstrating the beneficial effect of the additional glycosylation site on the stability of aggregation under the accelerated conditions. In addition, in terms of non-denatured productivity, R27T productivity was improved approximately 3~6 times more than that of rhIFN-β 1a under 30°C~34°C low temperature condition for 6~14 days, except for additional manipulation with a low-temperature adopted cell, using cytopore, intermediate temperature shift and perfusion for production (Table 4). It was assumed that it was due to the less aggregative properties conferred by additional glycosylation, because it was well known that the low productivity of rhIFN-β 1a was primarily attributed to molecular

aggregation.

The spatial coordinates of a R27T/IFNAR2 docking through computational simulation were determined to investigate the effect of glycosylation at residue 25. Glycosylation at residue 25 resulted in additional hydrogen bonding with 35R on R27T, improving the intrinsic stability. Moreover, structural simulation of R27T/IFNAR2 suggested that glycan moiety also interacted with IFNAR2, stabilizing the ligand-receptor binding interaction. These results implied that glycosylation could play an important role in fine-tuning the bioactivity of the glycoprotein, although X-ray crystallography experiments are required to obtain a more detailed structure [38].

Glycans have a very prominent role in affecting the therapeutic efficacy and *in vivo* half-life of recombinant proteins. The pharmacokinetic properties of R27T, its mixed form, and Rebif were compared. After IV administration, the pharmacokinetic parameters (CL, V_{ss}, and $t_{1/2}$) of Rebif (1 MIU/kg) in this study were consistent with those in a previous study regarding the pharmacokinetics of native rhIFN-β at a dose of 21 MIU/kg [14]. The AUC and CL values of R27T were significantly higher and lower, respectively, than those of Rebif and mixed R27T. Although little information regarding the route of elimination for rhIFN-β 1a is currently available, the reduced CL could be due to the fact that R27T is hyper-glycosylated rhIFN-β, in which the reduced CL could be attributed to molecular weight increase and/or sialylation status. It has also been reported that the CL of hyper-glycosylated erythropoietin is significantly lower than that of native

erythropoietin [39,40]. In this case, it has been documented that sialylation status is a critical attribute for pharmacokinetics [41,42]. In fact, the terminal monosaccharide of the N-linked complex glycan on R27T was occupied by sialic acid, which could affect absorption, serum half-life, and clearance, as well as physicochemical properties (manuscript in prep). Moreover, after SC and IM administration, the AUC and F values of R27T were significantly higher than those of Rebif and mixed R27T. This result could be attributed to the reduced CL and/or improved stability at the injection site of R27T as compared to Rebif. However, the exact reasons for enhanced SC and IM absorption and reduced elimination of R27T are unclear further investigation is required. Taken together, after IV, SC, and IM dosing to rats, R27T achieved enhanced and prolonged systemic rhIFN-β 1a exposure as compared to Rebif and mixed R27T, which could indicate the potential of R27T as a long-acting IFN analog.

Polyethyleneglycol (PEG) was conjugated to R27T to improve pharmacokinetic properties. After IV administration, the AUC, CL, and $t_{1/2}$ values of the PEG-R27Ts were significantly higher, lower, and longer, respectively, than those of R27T. These results suggested that PEG-R27T could enhance and prolong systemic exposure of IFN. Moreover, after SC and IM administration, the systemic exposure of IFN was significantly enhanced and prolonged in PEG-R27Ts. This result may be attributed to the reduced CL and/or prolonged absorption of PEG-R27Ts at the injection site due to their higher molecular weights relative to R27T. It is well known that PEGylated rhIFN-β formulations can provide prolonged and

enhanced systemic exposure of IFN in humans (Pegasys: PEGylated IFN-α-2a; PegIntron: PEGylated IFN-α-2b). Taken together, after IV, SC, and IM dosing in rats, PEG-R27Ts achieved enhanced and prolonged systemic IFN exposure compared with R27T, which indicates the potential of PEG-R27T as a long-acting IFN formulation.

VI. CONCLUSION

R27T displayed superior stability, solubility, and productivity, and had a reduced propensity for aggregation and an increased half-life without the loss of specific activity or alterations to ligand-receptor binding. PEG-R27T had a dramatically increased half-life. Hyperglycosylated or PEGylated rhIFN-β could be a biobetter version of rhIFN-β 1a with a potential for use as a drug against multiple sclerosis.

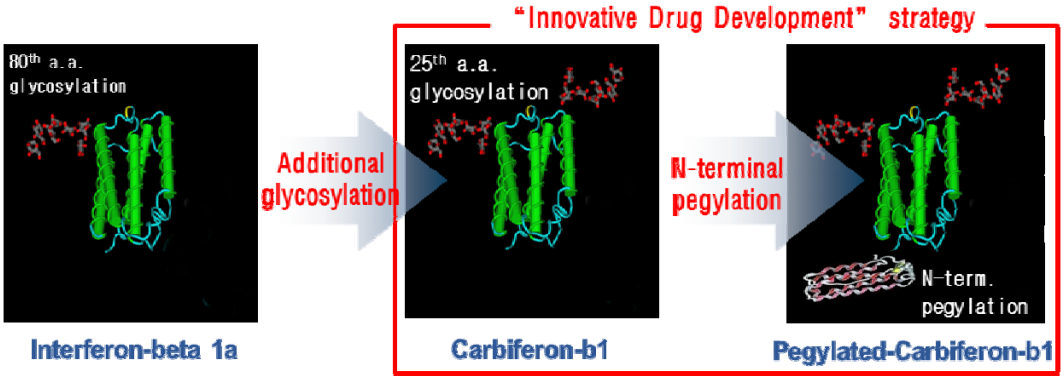

Figure 26. Innovative drug development strategy.

VII. REFERENCES

1. Noseworthy JH, Lucchinetti C, Rodriguez M, Weinshenker BG (2000) Multiple sclerosis. N Engl J Med 343: 938-952.
2. Fitzner D, Simons M (2010) Chronic progressive multiple sclerosis - pathogenesis of neurodegeneration and therapeutic strategies. Curr Neuropharmacol 8: 305-315.
3. Amedei A, Prisco D, D'Elios MM (2012) Multiple sclerosis: the role of cytokines in pathogenesis and in therapies. Int J Mol Sci 13: 13438-13460.
4. Baneke P, Browne P, Thompson AJ, Taylor B, Battaglia M, et al. (2013) MSIF Atlas of MS Database Update: Multiple Sclerosis Resources in the World 2013. Multiple Sclerosis Journal 19: 652-652.
5. Compston A, Coles A (2008) Multiple sclerosis. Lancet 372: 1502-1517.
6. Virley DJ (2005) Developing therapeutics for the treatment of multiple sclerosis. NeuroRx 2: 638-649.
7. de Seze J, Borgel F, Brudon F (2012) Patient perceptions of multiple sclerosis and its treatment. Patient Prefer Adherence 6: 263-273.
8. Brinar VV, Barun B (2013) Challenges in multiple sclerosis; how to define occurence of progression. Clin Neurol Neurosurg 115 Suppl 1: S30-34.
9. Rudick RA, Cohen JA, Weinstock-Guttman B, Kinkel RP, Ransohoff RM (1997) Management of multiple sclerosis. N Engl J Med 337: 1604-1611.
10. Lopez-Diego RS, Weiner HL (2008) Novel therapeutic strategies for multiple sclerosis--a multifaceted adversary. Nat Rev Drug Discov 7: 909-925.
11. Castro-Borrero W, Graves D, Frohman TC, Flores AB, Hardeman P, et al. (2012) Current and emerging therapies in multiple sclerosis: a systematic review. Ther Adv Neurol Disord 5: 205-220.
12. Gasperini C, Ruggieri S (2011) Emerging oral drugs for relapsing-remitting multiple sclerosis. Expert Opin Emerg Drugs 16: 697-712.
13. Nicholas R, Giannetti P, Alsanousi A, Friede T, Muraro PA (2011) Development of oral immunomodulatory agents in the management of multiple sclerosis. Drug Des Devel Ther 5: 255-274.

14. Pepinsky RB, LePage DJ, Gill A, Chakraborty A, Vaidyanathan S, et al. (2001) Improved pharmacokinetic properties of a polyethylene glycol-modified form of interferon-beta-1a with preserved in vitro bioactivity. J Pharmacol Exp Ther 297: 1059-1066.
15. Derynck R, Remaut E, Saman E, Stanssens P, De Clercq E, et al. (1980) Expression of human fibroblast interferon gene in Escherichia coli. Nature 287: 193-197.
16. Mark DF, Lu SD, Creasey AA, Yamamoto R, Lin LS (1984) Site-specific mutagenesis of the human fibroblast interferon gene. Proc Natl Acad Sci U S A 81: 5662-5666.
17. Kagawa Y, Takasaki S, Utsumi J, Hosoi K, Shimizu H, et al. (1988) Comparative study of the asparagine-linked sugar chains of natural human interferon-beta 1 and recombinant human interferon-beta 1 produced by three different mammalian cells. J Biol Chem 263: 17508-17515.
18. Antonetti F, Finocchiaro O, Mascia M, Terlizzese MG, Jaber A (2002) A comparison of the biologic activity of two recombinant IFN-beta preparations used in the treatment of relapsing-remitting multiple sclerosis. J Interferon Cytokine Res 22: 1181-1184.
19. Runkel L, Meier W, Pepinsky RB, Karpusas M, Whitty A, et al. (1998) Structural and functional differences between glycosylated and non-glycosylated forms of human interferon-beta (IFN-beta). Pharm Res 15: 641-649.
20. Baker DP, Pepinsky RB, Brickelmaier M, Gronke RS, Hu X, et al. (2010) PEGylated interferon beta-1a: meeting an unmet medical need in the treatment of relapsing multiple sclerosis. J Interferon Cytokine Res 30: 777-785.
21. Karpusas M, Nolte M, Benton CB, Meier W, Lipscomb WN, et al. (1997) The crystal structure of human interferon beta at 2.2-A resolution. Proc Natl Acad Sci U S A 94: 11813-11818.
22. Pettersen EF, Goddard TD, Huang CC, Couch GS, Greenblatt DM, et al. (2004) UCSF Chimera--a visualization system for exploratory research and analysis. J Comput Chem 25: 1605-1612.
23. Sanner MF, Olson AJ, Spehner JC (1996) Reduced surface: an efficient way to compute molecular surfaces. Biopolymers 38: 305-320.
24. Kirschner KN, Woods RJ (2001) Quantum mechanical study of the nonbonded

forces in water-methanol complexes. J Phys Chem A 105: 4150-4155.
25. Basma M, Sundara S, Calgan D, Vernali T, Woods RJ (2001) Solvated ensemble averaging in the calculation of partial atomic charges. J Comput Chem 22: 1125-1137.
26. Kirschner KN, Woods RJ (2001) Solvent interactions determine carbohydrate conformation. Proc Natl Acad Sci U S A 98: 10541-10545.
27. Quadt-Akabayov SR, Chill JH, Levy R, Kessler N, Anglister J (2006) Determination of the human type I interferon receptor binding site on human interferon-alpha2 by cross saturation and an NMR-based model of the complex. Protein Sci 15: 2656-2668.
28. Hornak V, Abel R, Okur A, Strockbine B, Roitberg A, et al. (2006) Comparison of multiple Amber force fields and development of improved protein backbone parameters. Proteins 65: 712-725.
29. Yoon I, Han S, Choi YH, Kang HE, Cho HJ, et al. (2012) Saturable sinusoidal uptake is rate-determining process in hepatic elimination of docetaxel in rats. Xenobiotica 42: 1110-1119.
30. Kim JE, Cho HJ, Kim JS, Shim CK, Chung SJ, et al. (2013) The limited intestinal absorption via paracellular pathway is responsible for the low oral bioavailability of doxorubicin. Xenobiotica 43: 579-591.
31. D GMaP (1982).
32. Yang CH, Wu PC, Huang YB, Tsai YH (2004) A new approach for determining the stability of recombinant human epidermal growth factor by thermal Fourier transform infrared (FTIR) microspectroscopy. J Biomol Struct Dyn 22: 101-110.
33. Dong A, Prestrelski SJ, Allison SD, Carpenter JF (1995) Infrared spectroscopic studies of lyophilization- and temperature-induced protein aggregation. J Pharm Sci 84: 415-424.
34. Fan H, Ralston J, Dibiase M, Faulkner E, Middaugh CR (2005) Solution behavior of IFN-beta-1a: an empirical phase diagram based approach. J Pharm Sci 94: 1893-1911.
35. Hubbard SJT, J.M. (1993) NACCESS. Computer Program, Department of Biochemistry and Molecular Biology, University College London.
36. Runkel L, Pfeffer L, Lewerenz M, Monneron D, Yang CH, et al. (1998) Differences in activity between alpha and beta type I interferons explored by

mutational analysis. J Biol Chem 273: 8003-8008.
37. Runkel L, deDios C, Karpusas M, Betzenhauser M, Muldowney C, et al. (2000) Systematic mutational mapping of sites on human interferon-beta-1a that are important for receptor binding and functional activity. Biochemistry 39: 2538-2551.
38. Knight P (1989) The Carbohydrate Frontier. Bio-Technology 7: 35-&.
39. Wanic-Kossowska M, Tykarski A, Kobelski M, Czekalski S (2006) [Effectiveness of darbepoietin alfa in anemic patients with chronic kidney disease (CKD) in predialysis period]. Pol Arch Med Wewn 116: 663-670.
40. Fang YW, Chang CH (2009) Subcutaneous administration of darbepoetin alfa effectively maintains hemoglobin concentrations at extended dose intervals in peritoneal dialysis patients. Perit Dial Int 29: 199-203.
41. Walsh G, Jefferis R (2006) Post-translational modifications in the context of therapeutic proteins. Nat Biotechnol 24: 1241-1252.
42. Delorme E, Lorenzini T, Giffin J, Martin F, Jacobsen F, et al. (1992) Role of glycosylation on the secretion and biological activity of erythropoietin. Biochemistry 31: 9871-9876.

VIII. 국 문 초 록

본 연구의 목적은 다발성경화증 치료제로 사용되고 있는 recombinant human interferon-β 1a (rhIFN-β 1a)의 biobetter version을 개발하기 위한 합리적 설계 및 이를 바탕으로 단백질 공학을 통해 rhIFN-β 1a의 생물리학적 성질 및 약동력학적 성질을 개선하는데 있다. rhIFN-b 1a는 80번째 아미노산에 당화를 가지고 있는 단백질로 높은 소수성의 성질로 인해 aggregation 현상이 강하게 나타나며 이러한 aggregation이 인터페론의 생물학적 활성을 줄이고 CHO 에서 단백질 생산의 수율을 낮추는 요인으로 작용한다고 알려져 왔다. 또한 인터페론은 상대적으로 적은 체내 반감기 때문에 빈번한 주사를 필요로 하며 이는 국소적인 피부발진을 야기하고 있다. 본 연구는 이러한 전반적인 인터페론 베타의 문제를 해결하고자, 합리적 설계에 따른 단백질 공학을 통해 당화 및 페길화를 도입하였다. 우선 당화를 유도하고자 구조 기능연구를 수행하였으며 이를 바탕으로 consensus 시퀀스로 가능한 site를 선별, site-direct mutagenesis를 통해 당화를 시도하였다. 그 결과 27번째 아미노산인 Arginine을 Threonine으로 치환시켰을 때 (R27T) 25번째 아미노산에 당화가 유도됨을 size의 증가로써 확인

하였다. 추가적으로 당화에 의한 charge varient를 IEF를 통해서 확인할 수 있었다. 이러한 단백질의 변형은 new molecular entity (NME)를 만들었고 이는 향상된 생산수율 및 aggregation 경향의 감소의 효과를 보였다. 당화는 비활성의 손실없이 생산성 및 단백질 안정성에 기여하는 것을 확인할 수 있었다. 그러나 체내 반감기에서 명확한 향상을 보여주지 않았으며 이를 보완하기 위해 R27T에 페길화를 수행하였다. 페길화 site 및 크기, liker의 종류 따라 페길화 효율 및 단백질의 비활성을 확인하였다. N-termimal 20kDa PEGylation을 최종 후보물질로 선정 체내 반감기를 확인한 결과 단백질의 체내 반감기를 극적으로 향상시킴을 확인하였다.

따라서 당화 및 페길화를 통한 단백질 공학기술을 이용한 rhIFN-b 1a의 biobetter 버전은 다발성경화증의 치료제로써 가능성을 보여주었다.

주 요 어: Recombinant human Interferon-β1a (rhIFN-β 1a), Rational design, Glycosylation, Pegylation, engineering, Biobetter, Multiple Sclerosis (MS)